AN EXPERIMENTAL INVESTIGATION ON THE DISTRIBUTION OF THE AERODYNAMIC LOADS OVER THE STRUCTURAL MEMBERS OF AN INFLATABLE, HIGH ASPECT RATIO (5.4), ADVANCED CONCEPT PARAGLIDER

by

Royce A. Toni

Thesis submitted to the Graduate Faculty of the
Virginia Polytechnic Institute
in candidacy for the degree of
MASTER OF SCIENCE
in
ENGINEERING MECHANICS

APPROVED: _____

_____ _____

_____

January 1967

Blacksburg, Virginia

II. TABLE OF CONTENTS

III. LIST OF FIGURES AND TABLES

FIGURE PAGE

FIGURE PAGE

TABLE PAGE

IV. INTRODUCTION

From the time the paraglider was first conceived, it has been the subject of an intense research effort. The interest generated for this aerodynamic gliding wing can be contributed to the fact that it provides what is a potentially feasible means for returning aerospace vehicles to earth in that it offers the capability of controlled touchdown at predetermined land sites. It does this by providing a relatively large lift-to-drag ratio as opposed to that of the parachute. The resulting increased glide and maneuvering capability can be controlled by the adjustment of the shroud line lengths. This in turn locates the payload relative to the resultant aerodynamic lift vector.

In this paper, interest is confined to the inflatable, advanced concept—high-aspect-ratio paraglider. This paraglider, which is packaged and stowed in a manner similar to that of the parachute, once deployed and pressurized takes on the shape illustrated in figure 1. The leading edges and keel, joined at the apex, serve as the structural members. They assume and maintain their respective shapes owing to the inflation pressure contained by their surfaces. The longitudinal shape of the leading edge centerline is curved, approximating an arc of a circle, while its circular cross section varies linearly from a relatively large diameter at the apex to a small diameter at the tip. The keel is considerably shorter in length and maintains a constant diameter circular cross section. The membrane is attached between the leading edges and keel.

Physically the membrane is entirely flexible and assumes a shape governed by the aerodynamic pressure.

Of paramount importance for controlled paraglider touchdown capability is the necessity to guarantee that first, upon deployment and inflation, the paraglider remains structually proficient and secondly, that it achieves the aerodynamic shape which yields the desired lift-to-drag ratio. In order to meet the above two requirements, a somewhat good knowledge of the aerodynamic load distribution over the structural members is essential. The complexity of achieving this can be contributed to two primary factors, they being; first, the interdependence of the shape of the membrane sail and the aerodynamic pressure and secondly, the leading edge geometry.

In reference 1 the problem is treated very nicely for the conventional concept paraglider. That is, the structural members are of equal length and lie in the same plane, thus no curved leading edge. In addition, the structural members are all assumed of negligible cross section with regards to direct aerodynamic effects. Reference 2 treats the problem of the high-aspect ratio paraglider, but it considers the case of the structural members being contained in the same plane. Thus, it also treats the leading edge as being straight. In addition, it also assumes the effects of the air pressure over the structural members as negligible.

Because a rigorous analysis is not within the present state-of-the-art, an experimental program was initiated at Langley Research Center incorporating the use of a series of load recording balances

in order to achieve some "feel" for the air load distributions over the structural members owing to the effects of aerodynamic pressure acting upon both the membrane sail and over the relatively large leading edge. The testing performed under this program is unique in that it is the only one of its kind known to date.

In order to establish the load ranges for the design of the load balances, an engineering theory had to be developed with respect to the air load distribution to the structural members. Since the purpose for this theory was primarily to estimate loads in an expediant manner, there was no need for a rigorous development.

It was believed that a comparison between the engineering theory and the experimental results would reveal similarities. However, it was found that for a reasonable comparison a rigorous analysis on the order of that contained in reference 1 would be essential. Since this is definitely beyond the scope of the paper herein, only the experimental results are presented.

These results in themselves demonstrate conclusively the order of magnitude of the distributed air loads over the structural members. In addition they yield a fairly good indication of the shape of the load distribution.

V. LIST OF SYMBOLS

A	subscript referring to leading edge reference system in a direction along the x_L - axis
AR	aspect ratio = $\frac{(2l_s)^2}{S_F}$
C	when followed by a subscript, refers to a coefficient with respect to that subscript; when used as a subscript, refers to the capsule
D	drag force on the paraglider
F	force acting over the structural members
F_{K_x}, F_{K_y}, F_{K_z}	components of resultant force of membrane tension on keel in x, y, and z directions, respectively
$F_{L_{A_{x_L}}}$	component of resultant force on leading edge in x_L direction
$F_{L_{A_\phi}}$	component of resultant force of membrane tension on leading edge in direction that makes the angle ϕ with x_L - axis
F_{L_I}	component of resultant force on leading edge that lies in x - y - plane and acts normal to leading edge = $F_{L_{I_\phi}}$
F_{L_z}	component of resultant force of membrane tension and direct aerodynamic effects on leading edge in direction

$F_{L_{q_z}}$	component of resultant force of direct aerodynamic effects on leading edge in z direction
$F_{L_{q_I}}$	component of resultant force of direct aerodynamic effects on leading edge that lies in x - y - plane and acts normal to leading edge
I	subscript referring to a direction normal to the x_L - axis and contained within the x - y - plane
K	subscript that refers to keel
l_K	loaded keel length
$l_{K_{\text{¢}}}$	keel centerline length
l_L	loaded leading edge length
$l_{L_{\text{¢}}}$	leading edge centerline length
L	lift force on paraglider; when used as subscript or when subscript refers to leading edge
L_{EK}, L_K, L_L	refer to figure 10
M	bending moment acting over structural members
M_K	bending moment acting over keel in x - z - plane
M_L	bending moment acting over leading edge in x_L - z - plane
M_{L_I}	bending moment acting over leading edge in x_L - x - plane
n	paraglider wing loading
N_{P_z}	total normal force acting on paraglider, normal to keel and in z direction

N_{L_ϕ} component of resultant force of combined membrane tension and direct aerodynamic effects on leading edge in direction that makes the angle ϕ with x_L - axis

P subscript refers to paraglider

q aerodynamic pressure

R resultant air load

S_F flat plan projected area of paraglider

T_{L_ϕ} component of resultant torsion of membrane tension on leading edge with respect to axis system rotated away from x_L - axis by angle ϕ

W_T weight of combined paraglider and capsule

$\frac{W_T}{S_p}$ paraglider wing loading

$w_N(x)$ running load owing to membrane tension distributed over keel in z - x - plane expressed as function of x

$w_N(\xi)$ running load from combined membrane tension and direct aerodynamic effects distributed over leading edge in x_L - z - plane expressed as function of ξ

$w_{N_q}(\xi)$ running load from direct aerodynamic effects only, distributed over leading edge in x_L - z - plane expressed as function of ξ

$x_{N_m}(\xi)$ running load from membrane tension only, distributed over leading edge in x_L - z - plane expressed as function of ξ

X_{p_x} total force acting on paraglider in x direction

x_L leading edge reference axis lying in x - y - plane

$\bar{x}$ arbitrary term to establish dimensionless moment coefficients (see appendix A, part 2)

x, y, z rectangular cartesian corrdinate in which x intersects the airstream by the angle α and the x - y - plane is in the vertical plane of symmetry of the paraglider

$\bar{x}_K$ point of action of $2F_{K_z}$

$\bar{x}_L$ point of action of F_{L_z}

α angle of attack of keel

δ_L angle made by intersection of leading edge and keel centerlines

λ angle made by the intersection of the paraglider total normal force and the resultant air load

γ angle made by intersection of lines of action of resultant air load and drag force

Λ sweep angle

ϕ axis system rotated away from x_L - axis by angle ϕ

ξ dummy variable representing arbitrary point on the leading edge reference system

VI. LOAD DEFINITION

Figure 2 depicts the coordinate system used in order to define the air load at some arbitrary point along any of the structural members. Owing to the symmetry about the paraglider's keel centerline, only that protion falling in the first quadrant need be considered.

The horizontal reference plane is defined as that plane containing the x and y ordinates. The leading edge reference system is the x_L - axis, and it lies in the x - y - plane. An arbitrary point along the leading edge reference system is designated ξ.

In referring to figure 3, the tension in the membrane (owing to the aerodynamic pressure exerted upon it) is resisted along both the leading edge and keel. The components of this tension load are depicted as F_{L_z}, $F_{L_{A_{x_L}}}$, and F_{L_I} for the leading edge; for the keel they are depicted as $2F_{K_z}$ and $2F_{K_x}$. All of these components are shown as the resultant forces applied directly to the structural members. In addition the leading edge, owing to its relatively large cross section, offers resistance to the aerodynamic pressure acting directly upon it. The component resultant loads for this resistant force are shown as $F_{L_{q_z}}$ and $F_{L_{q_I}}$.

Each resultant load is distributed along the structural member in its respective plane, and this distribution is a function of ξ for the leading edge and x for the keel. Forces acting on the keel in the horizontal reference plane cancel owing to symmetry. Keel

resistance to aerodynamic pressure is assumed negligible based upon its relatively small cross section.

VII. EXPERIMENTAL INVESTIGATION

Test Model

The paraglider shape under investigation in this paper was arrived at based upon the results of intensive aerodynamic research in the Langley Research Center 300 mph, 7- by 10-foot wind tunnel.[1] Once the shape which yielded the most favorable aerodynamic performance was established, a model was constructed. Its only purpose was for testing in the wind tunnel in order to record the air load distribution over its structural members. The important aerodynamic characteristics associated with the particular shape demonstrated by the model are:

(1) The resulting aspect ratio is approximately 5.45.

(2) The ratio of leading edge length to apex diameter is approximately 12.5.

(3) The dihedral angle is zero degrees, that is, the leading edge tip lies in the horizontal reference plane.

Unique geometrical characteristics associated with this shape are the circular arc generated by the leading edge length as well as its varying circular cross section. The membrane was a dacron sail cloth, weighing 4.8 oz/yd^2 and providing porosity sufficient to offer resistance to the tunnel air flow.

The model's structural members were rigid. The keel was fabricated from a two-inch diameter steel tube with facilities at the apex end for inserting a load balance. The two leading edges were

---

[1]The results of this research effort will be published at a later date as a NASA-TN authored by Paul G. Fournier.

fabricated differently from each other since there was no need for recording air load distributions over both members owing to the paraglider's symetrical geometry about its keel centerline. As a result only one leading edge incorporated the load recording balances. Figure 4 depicts the test model, and is complete only insofar as to provide the reader a basic concept of the model's structure. Figure 5 is a photograph of the model's internal mechanisms, and depicts more clearly the construction of both leading edges as well as the keel.

Load Recording Balances

There were five load recording balances utilized within the test model. Balance No. 1 was located at the leading edge apex, and numbers 2, 3, and 4 along the leading edge, at one-quarter points. Balance No. 5 was located at the keel apex. Figure 6 is a photograph depicting more clearly the physical characteristics of these balances. No attempt will be made to provide an elaborate discussion concerning the balance mechanisms.

The balance at the keel apex recorded the coefficients for shears, bending moments and axial forces in both the horizontal reference plane and the x - z - plane. It was assumed these forces were the keel resistance to membrane tension owing to aerodynamic pressure.

The leading edge balances were located in a plane passing through the leading edge centerline normal to the horizontal reference plane. Because of the leading edge curvature, its recorded force coefficients

(for shears, bending moments, torque and axial effects) are with respect to an axis offset by an angle ϕ to the x - y - z - rectangular cartesian coordinate system. This is more clearly presented by referring to Figure 4 and noting, for example, that ϕ is 21.83° for balance No. 1.

Test Procedure

The model was tested in Langley's 7- by 10-foot wind tunnel facility. Test data was recorded for varying angles of attack and aerodynamic pressures; however, only that data for an aerodynamic pressure of 5 psf was worthy of consideration, since data for higher value aerodynamic pressures revealed inconsistencies. These inconsistencies were contributed to the extreme sensitivities of the balances, which at higher air pressures became inaccurate. In addition, the accuracy of the load range predicted by the engineering theory for the design of the balances was considerably poor. This then imposed a definite limitation on the range of tunnel q. This situation was surmised only after preliminary analysis of the test data revealed no similarities between it and the engineering theory.

With regards to angle of attack, previous aerodynamic research (see footnote 1) revealed that for this particular paraglider shape maximum lift-to-drag ratio was achieved at 23 degrees, while 15 degrees was the desirable angle of attack for a flare maneuver. As a consequence, only the test results for angles of attack of 15 and 23 degrees are considered in the application of model test data to prototype distributed loadings.

VIII. TEST RESULTS AND DISCUSSION

Figures 8 and 9 represent the quantitative results of the experimental investigation. It becomes more convenient to apply the loads model test data to a paraglider of prototype dimensions. By doing so, an air load distribution is arrived at for a ptototype paraglider based upon the quantitative results of the experimental investigation.

Appendix A, part 1 describes the manner in which the prototype geometry is established. Parts 2, 3, and 4 of the same appendix provide the necessary expressions, so that when applied within aerodynamic constraints, test data can be transformed to prototype air load distributions. Appendix B describes the mechanics involved in this process, of which the results are shown in figures 12 and 13 for both the glide and flare angles of attack, respectively.

In examining the results, figures 12(a) and 12(b) in addition to 13(a) and 13(b), depict the distribution of the normal and axial air loads over the keel for both glide and flare angles of attack. The normal loading distribution meets both the aerodynamic and bending moment requirements as shown in part 1 of appendix B. The keel axial loading is assigned a second order distribution. This is based upon the assumptions that the only load induced upon the keel results from its resistance to membrane pull-off, and that the membrane leaves the keel at a constant angle throughout the keel's length. As a result,

the keel axial load is totally a component of the membrane tension, as is the normal load, and is therefore assigned a second order distribution.

Figure 12(c) depicts the normal air load component distribution over the leading edge. From figure 3 it can be seen that the shape of this curve is the superposition of the distributions for $F_{L_{q_z}}$ and F_{L_z}. These distributions are not known since the load balances yield only data enabling the plot of their combined effects. Noting that the leading edge is relatively large toward the apex end, it can be assumed that the aerodynamic pressure acting directly upon it has a significant effect at this end. Thusly, the distribution of $F_{L_{q_z}}$ is assumed such that the larger portion is up on the front end of the leading edge. The figure below depicts the assumed shape of this distribution.

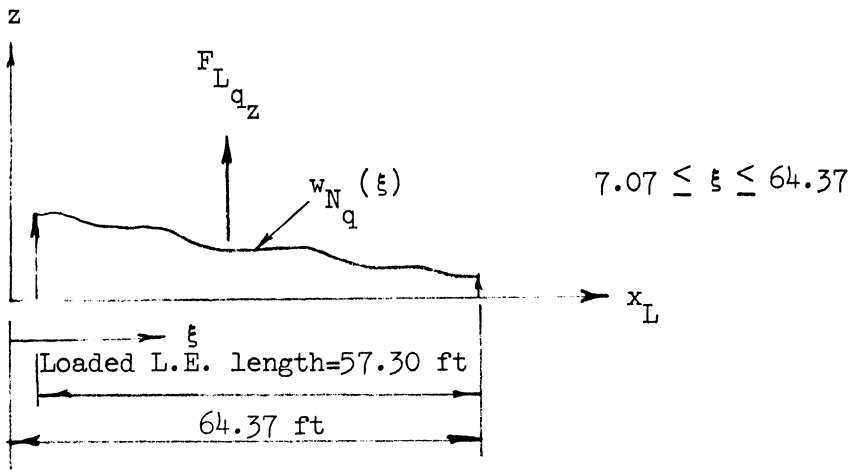

Since the leading edge length approximates a circular arc, the loading induced upon it owing to its resistance to membrane pull-off will undergo a change in direction. That is to say, its angle of pull-off is not constant. Thus the components of the membrane pull-off load are a function of this angle change. Also, at some point along the leading edge, the angle of pull-off is such that the membrane actually pulls off the leading edge in a direction down toward the keel. As a result, the component normal to the leading edge, that is F_{L_z}, can have a distribution assumed similar to that shown in the figure below:

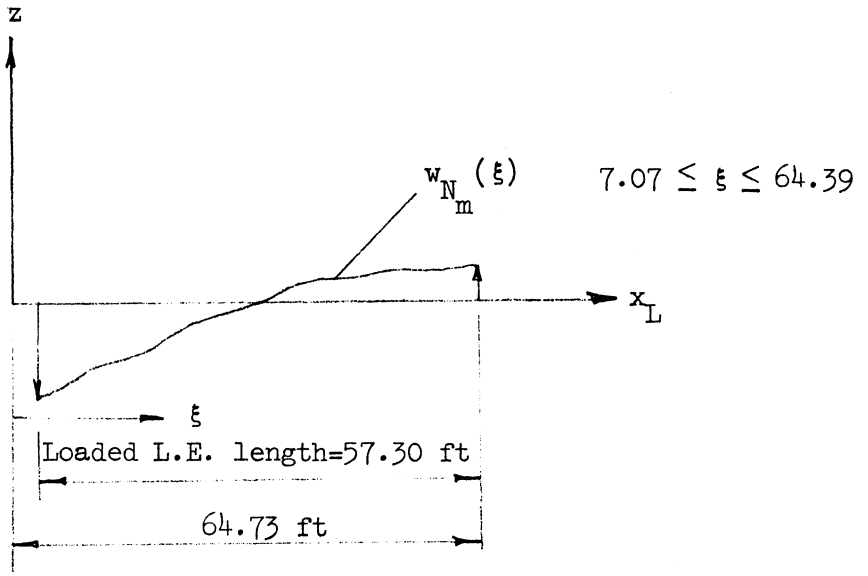

The superposition of the two preceeding load distributions can lead to the total load distribution shown in figure 12(c). The distribution shown in figure 13(c) can be justified similarly.

Figures 12(d) and 13(d) show the axially directed load component distribution over the leading edge for both glide and flare angles of

attack as second order distributions. This is based upon the assumptions that the axial loads are created only by membrane pull-off, and that the effects of the varying angle of pull-off are negligible with regards to load shape.

The curves shown as figures 12(e) and 13(e) represent the inboard air load component distribution over the leading edge for both glide and flare angles of attack. The curve of figure 12(e) meets the force and bending moment requirements stipulated upon it from the results of test data. The curve of figure 13(e) meets only the bending moment requirements.

It is interesting to note that the validity of the load curves presented herein can be substantiated by the results achieved under NASA contract NAS1-3020. Under this contract Goodyear Aerospace Corporation fabricated an inflatable, geometrically and elastically scaled, advanced concept paraglider model. It was wind tunnel tested at Langley, and preliminary results revealed lift to drag ratios of the order predicted by aerodynamic research. This then meant that the highly flexible model achieved a predicted shape.

Naturally the Goodyear model could not be fabricated to the dimensions it had to assume while in its operational glide mode, since owing to its flexibility, its structural members undergo rather large deflections. A deflection analysis was performed using the loads presented herein as the guidelines thereby enabling the establishment of fabrication dimensions. The fact that the model,

when wind tunnel tested, revealed predicted aerodynamic characteristics is indicative that the predetermined shape was achieved, which in turn substantiates the load guidelines.

IX. APPENDIX A

PARAGLIDER PROTOTYPE

1. Geometry

The exterior geometry of the paraglider prototype is a function of the total weight of the system and the allowable wing loading. The constituents of the system are the paraglider which represents 10 percent of the total weight and the capsule which accounts for the remaining 90 percent. This paper's interest in the advanced concept paraglider is confined to that of a recovery system for a space vehicle for which that system has assigned to it a total weight of 9200 pounds and a wing loading of 7 psf.

The expression for the paraglider flat projected area is defined as

$$S_F = \frac{W_T}{n} \tag{1}$$

Since the aspect ratio is defined as

$$AR = \frac{(2l_S)^2}{S_F} \tag{2}$$

the expression for the span length is

$$l_S = \sqrt{\frac{(AR)S_F}{4}} \tag{3}$$

From Trigonometry the flat projected area can be derived. It is expressed as

$$S_F = l_S L_K \tag{4}$$

from which

$$L_K = \frac{S_F}{l_S} \tag{5}$$

Again from Trigonometry the span length can be expressed as

$$l_S = L_E \cos \Lambda \tag{6}$$

which enables the solution of the leading-edge length:

$$L_E = \frac{l_S}{\cos \Lambda} \tag{7}$$

And finally,

$$L_{EK} = l_S \tan \Lambda \tag{8}$$

For this particular study

$$W_T = 9200 \text{ lbs} \tag{9}$$

$$n = 7 \text{ psf} \tag{10}$$

$$\Lambda = 50^\circ \tag{11}$$

When applied to the above equations the results are

$$S_F = 1314 \text{ ft}^2 \tag{12}$$

$$l_S = 42.1 \text{ ft} \tag{13}$$

$$L_K = 31.2 \text{ ft} \tag{14}$$

$$L_L = 65.5 \text{ ft} \tag{15}$$

$$L_{EK} = 50.2 \text{ ft} \tag{16}$$

2. Expressions for Force Coefficients

Expressions for the force coefficients are defined as

$$C_{N_{L_\phi}}, C_{A_{L_\phi}}, C_{F_{L_I}}, C_{2F_{K_z}}, C_{2F_{K_x}} = \frac{F}{qS_F} \tag{17}$$

where

$$F = N_{L_\phi}, F_{L_{A_\phi}}, F_{L_I}, 2F_{K_z}, 2F_{K_x} \tag{18}$$

And,

$$C_{M_{L_z}}, C_{M_{L_I}}, C_{T_{L_\phi}}, C_{M_{K_z}} = \frac{M}{qS_F\bar{x}} \tag{19}$$

where

$$M = M_L, M_{L_{I_\phi}}, T_{L_\phi}, M_K \tag{20}$$

The term $\bar{x}$ is arbitrary. Its purpose is to establish some reference in order to have a dimensionless moment coefficient. In the case of the loads model, $\bar{x}$ is a value of ξ at θ_L which extends 41.86 inches. Thus, we can find $\bar{x}$ for the prototype paraglider simply by using the expression

$$\bar{x}_{\text{Prototype}} = \left(\frac{\bar{x}}{L_E}\right)_{\text{Model}} \left(L_E\right)_{\text{Prototype}} \tag{21}$$

For the specific case under consideration herein,

$$\bar{x}_{\text{Prototype}} = 61.5 \text{ ft} \tag{22}$$

3. Expressions for the Transformation of the Recorded Leading Edge Force Coefficients to the Leading Edge

Figure 9(a) depicts the recorded force coefficients acting in their positive sense at some arbitrary point located on the leading edge centerline.

The following equations are applicable for transforming the above recorded load coefficients to the x_L - axis, which serves as the leading edge reference system.

$$C_{N_{L_z}} = C_{N_{L_\phi}} \cos \phi - C_{A_{L_\phi}} \sin \phi \tag{23}$$

$$C_{F_{L_{A_{x_L}}}} = C_{N_{L_\phi}} \sin \phi + C_{F_{L_{A_\phi}}} \cos \phi \tag{24}$$

$$C_{M_L} = C_{M_{L_\phi}} \tag{25}$$

$$C_{F_{L_I}} = C_{F_{L_{I_\phi}}} \tag{26}$$

$$C_{M_{L_I}} = C_{M_{L_{I_\phi}}} \cos \phi - C_{T_{L_\phi}} \sin \phi \tag{27}$$

$$C_{T_L} = C_{T_{L_\phi}} \cos \phi + C_{M_{L_{I_\phi}}} \sin \phi \tag{28}$$

The value of the angle ϕ for each load station along the leading edge centerline is shown in figure 4. For example ϕ at the location of balance No. 1 is 21.83°.

4. Aerodynamic Pressure for Prototype System

Since from definition

$$\frac{C_L}{C_D} = \frac{L}{D} \tag{29}$$

then for the paraglider alone,

$$C_{DP} = \frac{C_{LP}}{(L/D)_P} \tag{30}$$

For the system (paraglider and capsule)

$$\frac{L_S}{D_S} = \frac{L_P + L_C}{D_P + D_C} \tag{31}$$

But in general, from definition

$$L = C_L qS \tag{32}$$

and

$$D = C_D qS \tag{33}$$

Substituting equations (32) and (33) into (31) and canceling q yields

$$\frac{L_S}{D_S} = \frac{C_{LP}S_{FP} + C_{LC}S_C}{C_{DP}S_{FP} + C_{DC}S_C} \tag{34}$$

From definition

$$\gamma = \tan^{-1} \frac{L}{D} \tag{35}$$

therefore referring to figure 11, for the system,

$$\gamma_S = \tan^{-1} \frac{L_S}{D_S} \tag{36}$$

Now then the system's resultant force can be expressed as

$$R_S = \frac{L_S}{\sin \gamma_S} \tag{37}$$

For a specific angle of attack the lift of the system, L_S, can be represented as $C_1 q$ where C_1 is a constant. Thus,

$$R_S = \frac{C_1 q}{\sin \gamma_S} \tag{38}$$

But,

$$R_S \approx W_T \tag{39}$$

Therefore the expression for q becomes

$$q = \frac{W_T \sin \gamma_S}{C_1} \tag{40}$$

By using the aerodynamic characteristics listed under tables 2 and 3 and substituting into equations (29) through (40) in that order, q can be found for angles of attack of 15° and 23°. They become respectively

$$q = 8.06 \text{ psf} \quad \text{for} \quad \alpha = 15^\circ \tag{41}$$

$$q = 5.31 \text{ psf} \quad \text{for} \quad \alpha = 23^\circ \tag{42}$$

However, since $\alpha = 23^{\circ}$ represents the flare maneuver, the paraglider is undergoing a sudden acceleration and no longer is in a steady state glide flight mode. At this time, the structural members will be induced to their maximum loading. To account for this sudden acceleration, a load correction factor of $n = 1.5$ is applied to q. Thus,

$$q = 7.89 \text{ psf} \quad \text{for} \quad \alpha = 23^{\circ} \tag{43}$$

5. Calculation of N_{P_q} Based Upon Aerodynamic Characteristics

The expressions for the total aerodynamic component loads acting normal to and lying in the horizontal reference plane are, respectively given as

$$N_{P_z} = C_{NP} q S_F \tag{44}$$

$$X_{P_x} = C_{XP} q S_F \tag{45}$$

It is assumed that these components act at the paraglider center of pressure which in turn is located on the keel centerline. This is shown in figure 11.

From figure 11 it can be seen that

$$C_{NP} = C_{RP} \cos \lambda_P \tag{46}$$

From equation (35)

$$\gamma_P = \tan^{-1} \frac{L_P}{D_P} \tag{47}$$

Referring to figure 11

$$\lambda_P = \alpha_P + \tan^{-1} \frac{L_P}{D_P} - 90^\circ \tag{48}$$

Also

$$C_{RP} = \frac{C_{LP}}{\sin \gamma_P} \tag{49}$$

or,

$$C_{RP} = \frac{C_{LP}}{\sin\left[\tan^{-1} \frac{L_P}{D_P}\right]} \tag{50}$$

By substituting equations (47) and (50) into (46) the expression for C_{NP} becomes

$$C_{NP} = \frac{C_{LP}}{\sin\left[\tan^{-1} \frac{L_P}{D_P}\right]} \cos\left[\alpha_P + \tan^{-1} \frac{L_P}{D_P} - 90^\circ\right] \tag{51}$$

And finally the expression for N_{P_z} is arrived at by substituting equation (51) into (44).

$$N_{P_z} = \frac{C_{LP} \cos\left[\alpha_P + \tan^{-1} \frac{L_P}{D_P} - 90^\circ\right]}{\sin\left[\tan^{-1} \frac{L_P}{D_P}\right]} qS_F \tag{52}$$

For the particular case under consideration herein, the paraglider aerodynamic characteristics can be taken from table 2. The value of S_F has been arrived at and is listed as equation (12). The aerodynamic pressure for both glide and flare angles of attack are listed as equations (41) and (43). Therefore,

$$N_{P_z} = 8870 \text{ lbs} \quad \text{for} \quad \alpha_P = 15^\circ \tag{53}$$

$$N_{P_z} = 13{,}200 \text{ lbs} \quad \text{for} \quad \alpha_P = 23^\circ \tag{54}$$

X. APPENDIX B

PROTOTYPE AIR LOAD DISTRIBUTION BASED UPON EXPERIMENTAL INVESTIGATION

This appendix concerns itself with the mechanics involved in the use of test data from the wind tunnel paraglider model to arrive at the distributed air loadings for a prototype configuration. The procedure that follows is shown only for the case of a 15 degree glide angle of attack; however, the same procedure can be used for the flare angle of attack by substituting the appropriate data.

1. The Normal Air Load Component Distribution

The following constraint concerning the normal air load distribution must be met. That is,

$$2F_{K_z} + 2\left(F_{L_z} + F_{L_z}\right) = N_{P_z} \tag{55}$$

From equations (17) and (18) the expression for the normal air load acting on the keel is

$$2F_{K_z} = C_{2F_{K_z}}\, q\, S_F \tag{56}$$

Also from equations (17) and (18),

$$N_{L_\phi} = C_{N_{L_\phi}}\, q\, S_F \tag{57}$$

The expression for the air load normal to the leading edge reference system the $\left(x_L - \text{axis}\right)$ is given by

$$N_{L_z} = C_{N_{L_z}} \, q \, S_F \tag{58}$$

where from equation (23)

$$C_{N_{L_z}} = C_{N_{L_\phi}} \cos \phi - C_{A_{L_\phi}} \sin \phi \tag{59}$$

Substituting equation (59) into (58) results in

$$N_{L_z} = \left(C_{N_{L_\phi}} \cos \phi - C_{F_{L_{A_\phi}}} \sin \phi \right) q \, S_F \tag{60}$$

But,

$$N_{L_z} = \left(F_{L_z} + F_{L_{q_z}} \right) \tag{61}$$

Therefore,

$$\left(F_{L_z} + F_{L_{q_z}} \right) = \left(C_{N_{L_\phi}} \cos \phi - C_{A_{L_\phi}} \sin \phi \right) q \, S_F \tag{62}$$

Equation (56) when evaluated at balance No. 5, at which

$$C_{2F_{K_z}} = 0.40$$

and

$$q = 8.06 \text{ psf}$$

$$S_F = 1314 \text{ ft}^2$$

yields

$$2F_{K_z} = 4236 \text{ lbs} \tag{63}$$

which is the total normal keel air load.

Equation (62) when evaluated at balance No. 1 yields the total air load normal to the leading edge reference system. At balance No. 1

$$\phi = 21.83^\circ$$

$$C_{N_{L_\phi}} = .29$$

$$C_{A_{L_\phi}} = .27$$

and also

$$q = 8.06 \text{ psf}$$

$$S_F = 1314 \text{ ft}^2$$

Therefore,

$$\left(F_{L_z} + F_{L_{q_z}}\right) = 1790 \text{ lbs} \tag{64}$$

Referring to equation (53)

$$N_{P_z} = 8870 \text{ lbs}$$

Thusly, equation (55) becomes

$$2F_{K_z} + 2\left(F_{L_z} + F_{L_{q_z}}\right) = 8870 \text{ lbs} \tag{65}$$

and this restraint is met only if after substituting equations (63) and (64) into equation (65) the left hand side of the equation is multiplied by some factor k. Thus

$$k\left[4236 + 2(1790)\right] = 8870 \tag{66}$$

from which

$$k = 1.135 \tag{67}$$

Therefore, the results of equations (63) and (64) are adjusted by a factor of 1.135. This then yields

$$2F_{K_z} = 4808 \text{ lbs} \tag{68}$$

and

$$\left(F_{L_z} + F_{L_{q_z}}\right) = 2031 \text{ lbs} \tag{69}$$

From equations (19) and (20) the expression for the bending moment on the keel is

$$M_K = C_{M_K} \, q \, S_F \, \bar{x} \tag{70}$$

The above equation when evaluated at balance No. 5 results in the total keel bending moment. At balance No. 5

$$C_{M_K} = 0.035$$

and

$$q = 8.06 \text{ psf}$$

$$S_F = 1314 \text{ ft}^2$$

$$\bar{x} = 61.5 \text{ ft}$$

Applying the factor k of 1.135 to the result yields

$$M_K = 25{,}863 \text{ ft-lbs} \tag{71}$$

Therefore the load distribution over the keel can be depicted as that in the following figure:

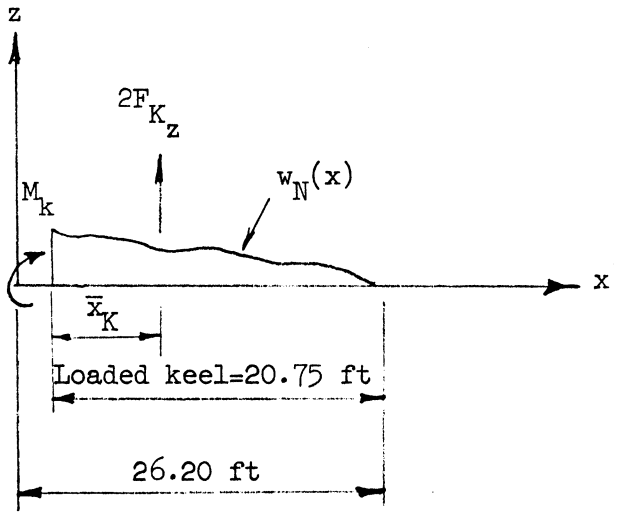

From the above figure,

$$\bar{x}_K = \frac{M_K}{2F_{K_z}} \tag{72}$$

Thus,

$$\bar{x}_K = 5.38 \text{ ft} \tag{73}$$

Since the ratio between $\bar{x}_K$ and the loaded keel length is

$$\frac{5.38}{20.75} \approx 0.25 \tag{74}$$

therefore the air load distribution for $2F_{K_z}$ is of the type

$$w_N(x) = \frac{w_o}{(20.75)^2} (26.2 - x)^2 \qquad 5.45 \leq x \leq 26.2 \tag{75}$$

To evaluate w_o, set

$$4808 = \frac{w_o}{(20.75)^2} \int_{5.45}^{26.2} (26.2 - x)^2 \, dx \tag{76}$$

from which

$$w_o = 693.2 \text{ lbs/ft} \tag{77}$$

Thus, equation (75) becomes

$$w_N(x) \times 1.61 (26.2 - x)^2 \tag{78}$$

This is shown as figure 12(a).

In considering the bending moment on the leading edge the effects of axially directed forces are assumed negligible. Thus, from equations (19) and (20)

$$M_L = C_{M_L} \, q \, S_F \, \bar{x} \tag{79}$$

where

$$C_{M_L} = C_{M_{L_\emptyset}} \tag{80}$$

Now equation (79) evaluated at balance No. 1 where

$$C_{M_L} = 0.12$$

and

$$q = 8.06 \text{ psf}$$

$$S_F = 1314 \text{ ft}^2$$

$$\bar{x} = 61.5 \text{ ft}$$

and corrected by the factor k of 1.135 yields

$$M_L = 88{,}712 \text{ ft-lbs} \tag{81}$$

The total distribution over the leading edge can therefore be depicted in the figure below:

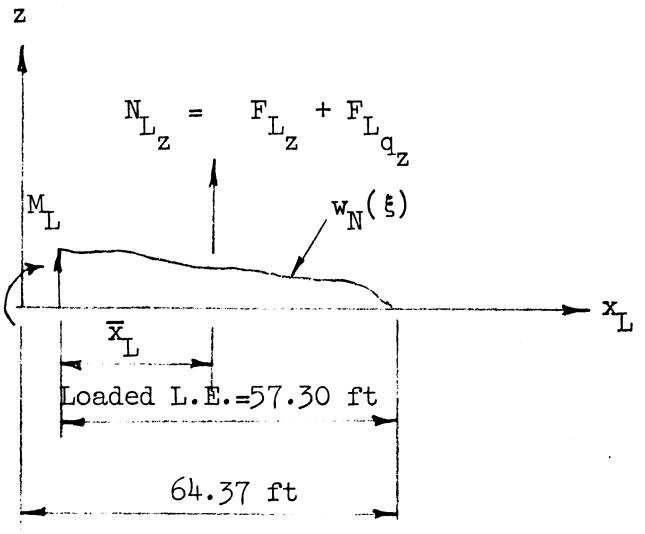

From the above figure,

$$\bar{x}_L = \frac{M_L}{N_{L_z}} \tag{82}$$

Thus

$$\bar{x}_L = 43.68 \text{ ft} \tag{83}$$

And the ratio between $\bar{x}_L$ and the loaded leading edge length is

$$\frac{43.68}{53.70} \approx 0.75 \tag{84}$$

This reveals that the air load distribution for N_{L_z} is of the type

$$w_N(\xi) = \frac{w_o}{(57.3)^2} (\xi - 7.07)^2 \qquad 7.07 \leq \xi \leq 64.37 \tag{85}$$

This is shown in figure 12(c), where w_o is evaluated to be 106.3 lbs/ft.

2. The Distribution of the Air Load Component Axially Directed to the Structural Members

From equations (17) and (18) the expression for the air load acting axial on the keel is

$$2F_{K_x} = C_{2F_{K_x}} q S_F \tag{86}$$

Also from equations (17) and (18)

$$F_{L_{A_\phi}} = C_{F_{L_\phi}} q S_F \tag{87}$$

The expression for the load acting axial on the leading edge with respect to the leading edge reference axis is

$$F_{L_{A_{x_L}}} = C_{F_{L_{A_{x_L}}}} q S_F \tag{88}$$

where from equation (24)

$$C_{F_{L_{A_{x_L}}}} = C_{N_{L_\phi}} \sin \phi + C_{F_{L_{A_\phi}}} \cos \phi \tag{89}$$

Thus, from substituting the above into equation (88) the following is established

$$F_{L_{A_{x_L}}} = \left(C_{N_{L_\phi}} \sin \phi + C_{F_{L_{A_\phi}}} \cos \phi \right) q S_F \tag{90}$$

Equation (87) when evaluated at balance No. 5 yields the total air load axial to the keel. At balance No. 5

$$C_{2F_{K_x}} = -0.34$$

and

$$q = 8.06 \text{ psf}$$

$$S_F = 1314 \text{ ft}^2$$

Therefore,

$$2F_{K_x} = -3600 \text{ lbs} \tag{91}$$

and the negative sign indicates the keel axial load is tension.

Equation (90) when evaluated at balance No. 1 results in the total leading edge air load directed axially to the leading edge with respect to the leading edge reference axis. At balance No. 1

$$\phi = 41.83^{\circ}$$

$$C_{N_{L_\phi}} = .29$$

$$C_{F_{L_{A_\phi}}} = .27$$

and also

$$q = 8.06 \text{ psf}$$

$$S_F = 1314 \text{ ft}^2$$

Thus,

$$F_{L_{A_{x_L}}} = 3780 \text{ lbs} \tag{92}$$

The results found in equations (91) and (92) must be adjusted by a factor of 1.135. Thusly,

$$2F_{K_x} = -4086 \text{ lbs tension} \tag{93}$$

and

$$F_{L_{A_{x_L}}} = 4290 \text{ lbs compression} \tag{94}$$

The above loads are distributed to the respective structural members in a second order fashion. Therefore, for the keel

$$w_A(x) = 1.37\ (26.2 - x)^2 \qquad 5.45 \leq x \leq 26.2 \tag{95}$$

and for the leading edge

$$w_A(\xi) = 0.069\ (64.37 - \xi)^2 \qquad 7.07 \leq \xi \leq 64.37 \tag{96}$$

These distributions are plotted in figures 12(b) and 12(d).

3. The distribution of the Air Load Component Lying in the Horizontal Reference Plane and Normal to the Leading Edge (Leading Edge Inboard Air Load Component)

Based upon equations (17) and (18), the expression for the air load lying in the horizontal reference plane and normal to the leading edge is

$$\left(F_{L_{I_\phi}} + F_{L_{q_I}}\right) = C_{F_{L_I}}\, q\, S_F \tag{97}$$

where

$$C_{F_{L_I}} = C_{F_{L_{I_\phi}}} \tag{98}$$

Equation (97) when evaluated at balance No. 1 results in the total air load lying in the horizontal reference plane and normal to the leading edge. At the location of balance No. 1

$$C_{F_{L_I}} = 0.03$$

and

$$q = 8.06 \text{ psf}$$

$$S_F = 1314 \text{ ft}^2$$

Applying the above to equation (98) and correcting by the k factor of 1.135 yields

$$\left(F_{L_I} + F_{L_{q_I}}\right) = 358 \text{ lbs} \tag{99}$$

From equations (19) and (20) comes

$$M_{L_{I_\phi}} = C_{M_{L_{I_\phi}}} q S_F \bar{x} \tag{100}$$

The expression for the bending moment in the horizontal reference plane that tends to pivot the leading edge about the apex and in toward the keel is

$$M_{L_I} = C_{M_{L_I}} q S_F \bar{x} \tag{101}$$

where

$$C_{M_{L_I}} = C_{M_{L_{I_\phi}}} \cos \phi - C_{T_{L_\phi}} \sin \phi \qquad (102)$$

Thus, equation (101) now becomes

$$M_{L_I} = \left(C_{M_{L_{I_\phi}}} \cos \phi - C_{T_{L_\phi}} \sin \phi \right) q \, S_F \, \bar{x} \qquad (103)$$

The above expression evaluated at balance No. 1, where

$$\phi = 21.83^\circ$$

$$C_{M_{L_{I_\phi}}} = .02$$

$$C_{T_{L_\phi}} = -.0035$$

and

$$q = 8.06 \text{ psf}$$

$$S_F = 1314 \text{ ft}^2$$

$$\bar{x} = 61.5 \text{ ft}$$

and the result corrected by the factor 1.135 yields the magnitude of the total bending moment. Thus,

$$M_{L_I} = 14{,}584 \text{ ft-lbs} \qquad (104)$$

The distribution of $\left(F_{L_I} + F_{L_{q_I}}\right)$ that will satisfy the above moment restraint is assumed linear and is arrived at by trial and error. This distribution is shown in figure 12(e).

XI. ACKNOWLEDGEMENTS

The author wishes to express his appreciation to the National Aeronautics and Space Administration for the use of its facilities. Special gratitude is conveyed to James F. McNulty for his encouragement and advice in developing structural design approaches for the paraglider. Sincere appreciation is extended to the author's wife for her patience.

XII. REFERENCES

1. Fralich, Robert W.: Stress and Shape Analysis of a Paraglider. Thesis submitted to the Graduate Faculty of the Virginia Polytechnic Institute in candidacy for the degree of Doctor of Philosophy in Engineering Mechanics. June 1963.

2. Kriebel, A. R.; and Nielsen, J. N.: Theoretical Aerodynamics of Flexible Wings at Low Speeds, III - Approximate Results for Wings of Large Aspect Ratio. Prepared for Air Programs Office of Naval Research, Washington, D. C. Vidya Project No. 9064, Vidya Report No. 146, July 1964.

3. Hoffman, T. L.; and Raff, B. W.: Advanced Concept Inflatable Paraglider Prototype and Model Design. Contract No. NAS 1-3020 May 15, 1964. pp. 3-7.

4. Toni, Royce A.; and McNulty, James F.: Design Criteria for Inflated, Expandable Beams Used as Structural Members in an Advanced Concept Paraglider. Presented at the Second Aerospace Expandable Structures Conference in Minneapolis, Minnesota, May 1965.

The vita has been removed from the scanned document

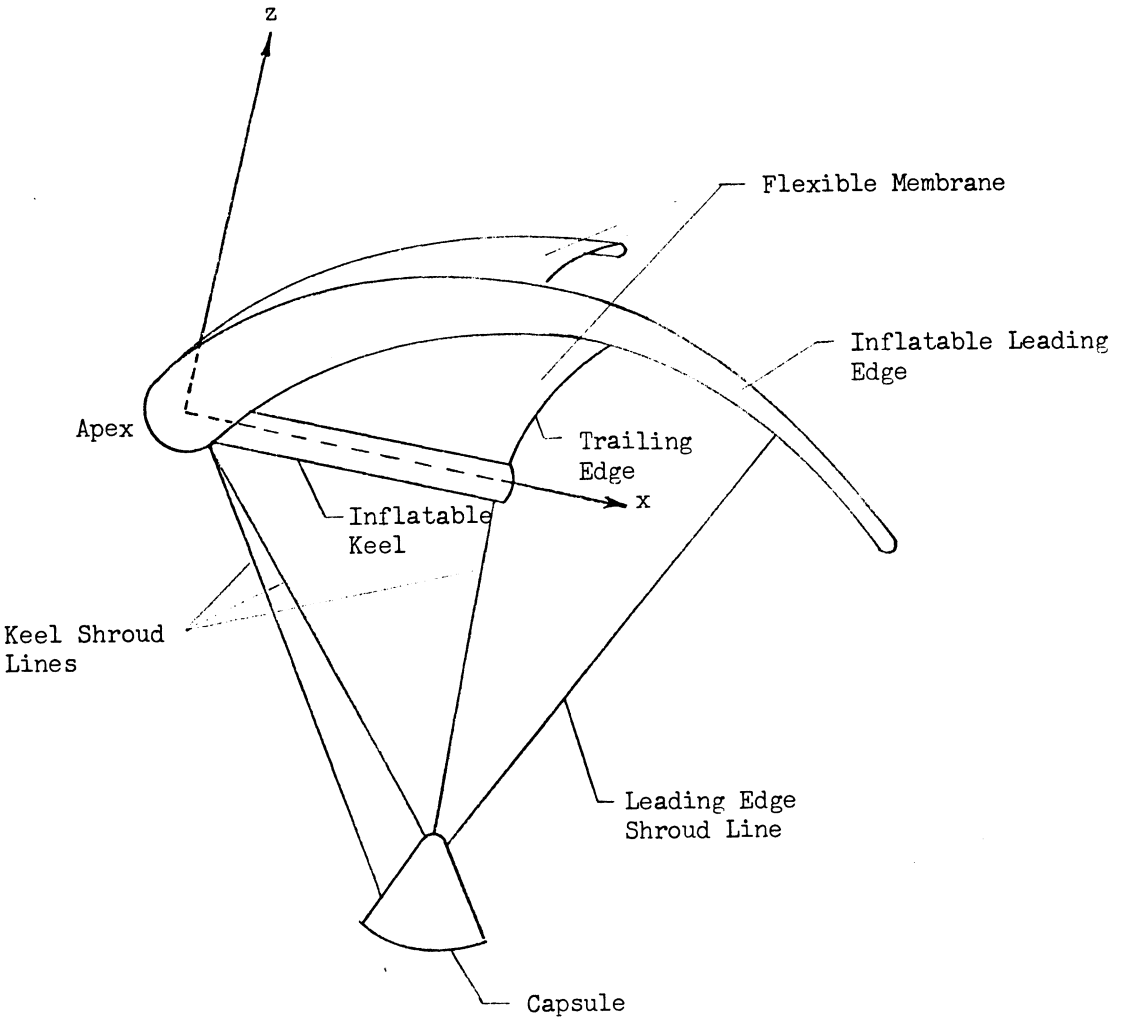

Figure 1.- A deployed, inflated advanced concept paraglider with suspended capsule.

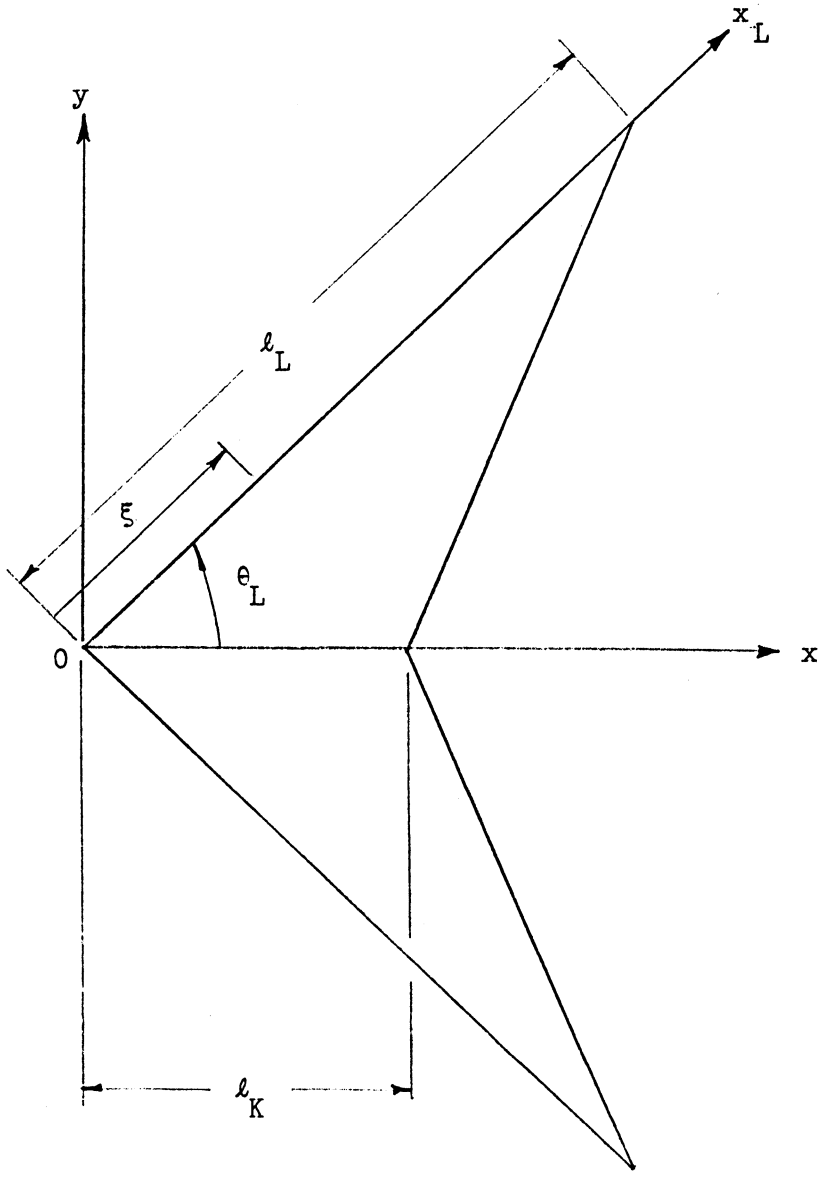

Figure 2.- Coordinate system where x - y - axis represents horizontal reference plane, and the x_L - axis, lying in this plane represents the leading edge reference system.

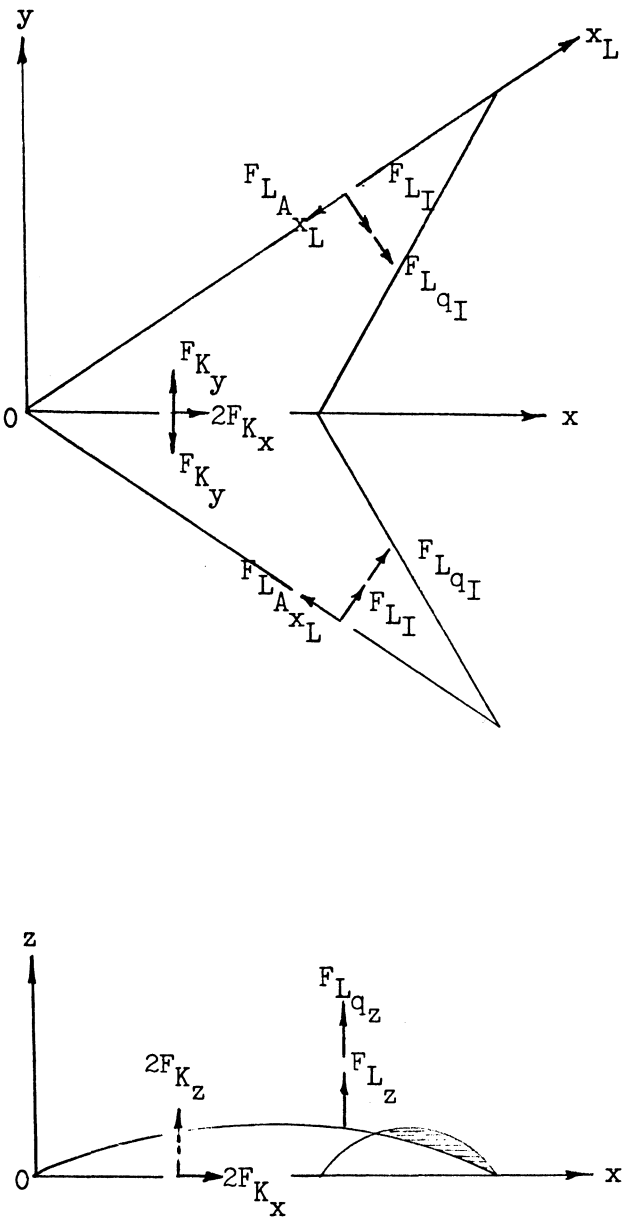

Figure 3.- Resultant forces (shown in their positive sense) applied to the structural members.

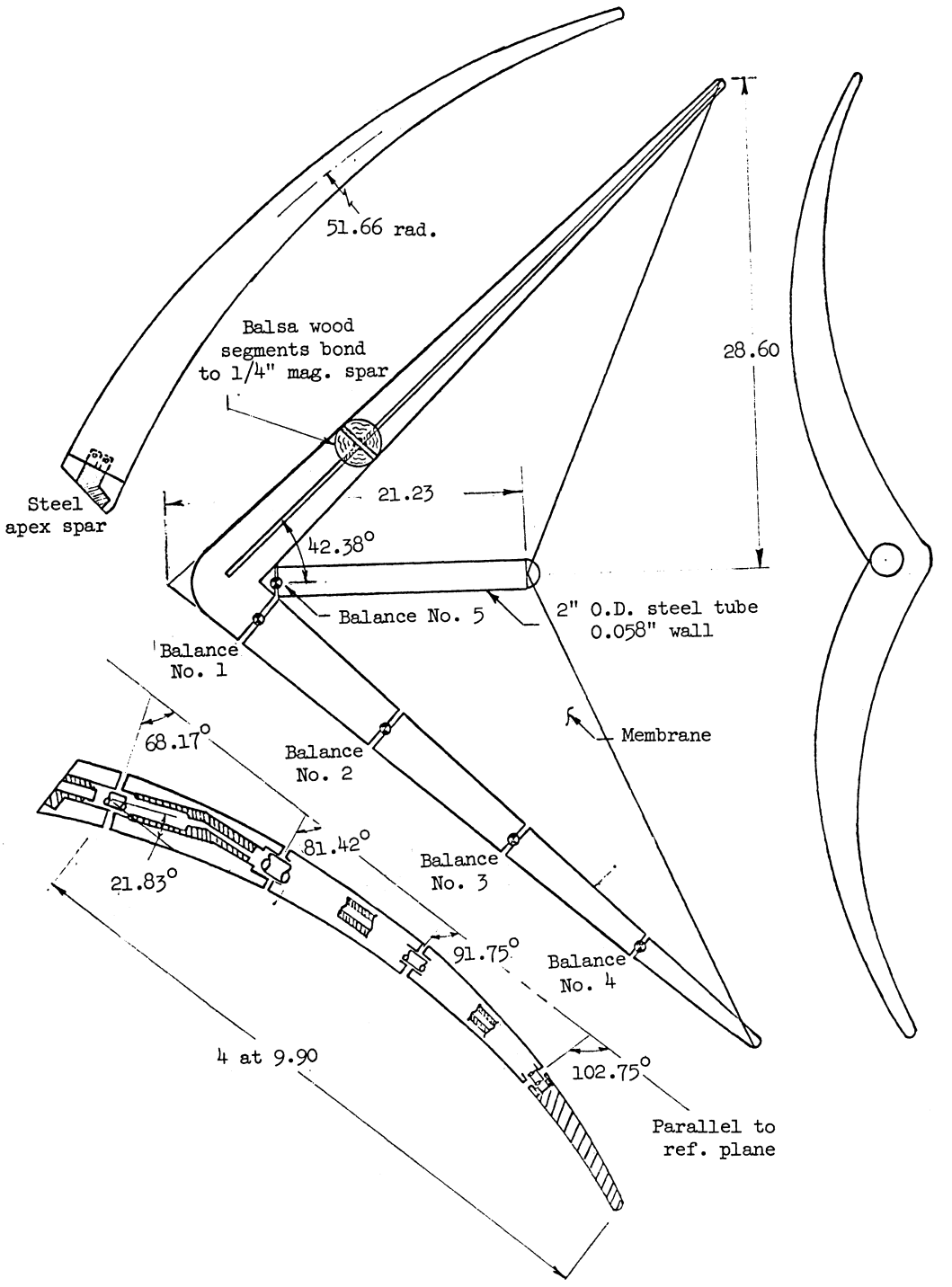

Figure 4.- The advanced concept paraglider loads test model (all dimensions shown in inches).

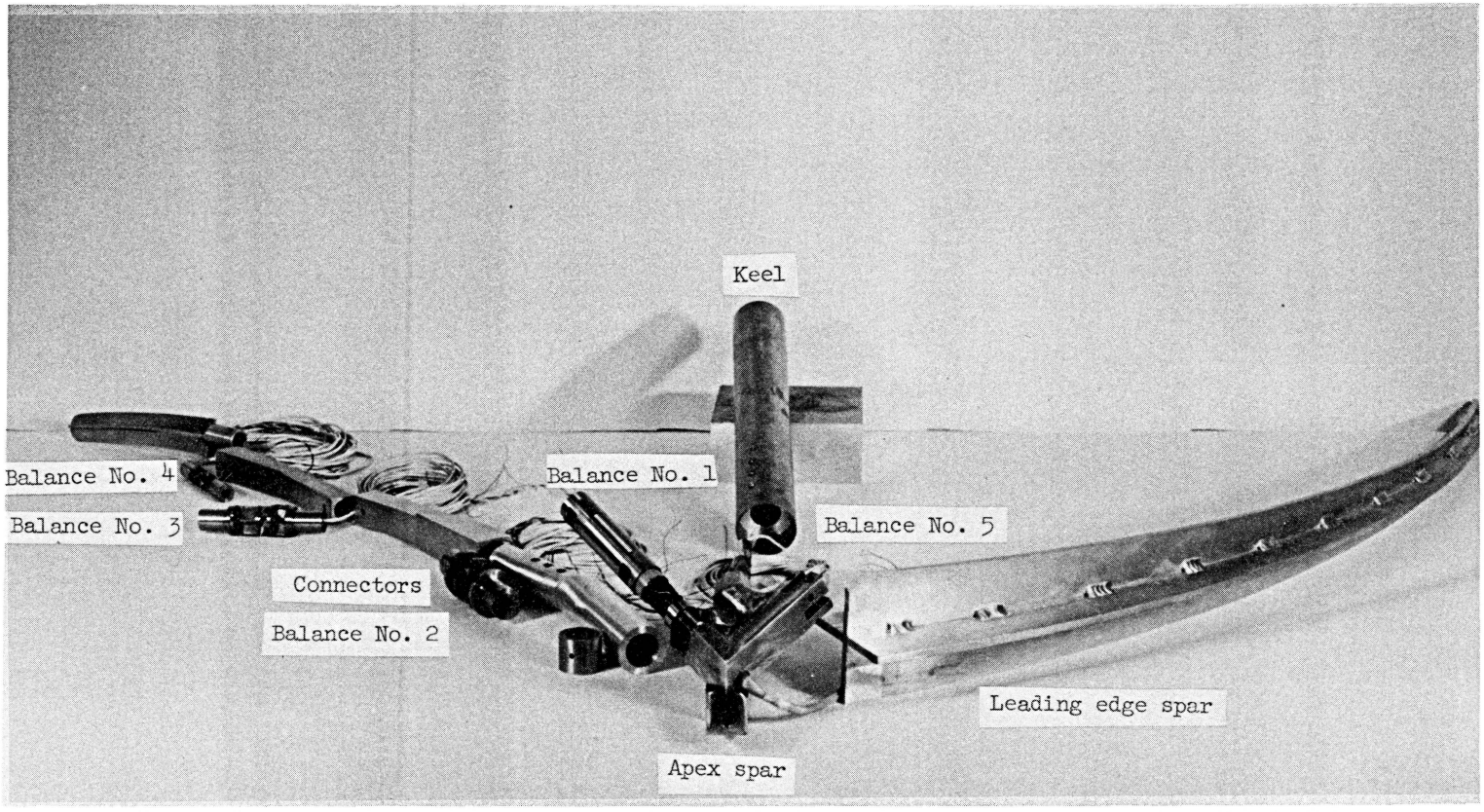

Figure 5.- Test model internal components.

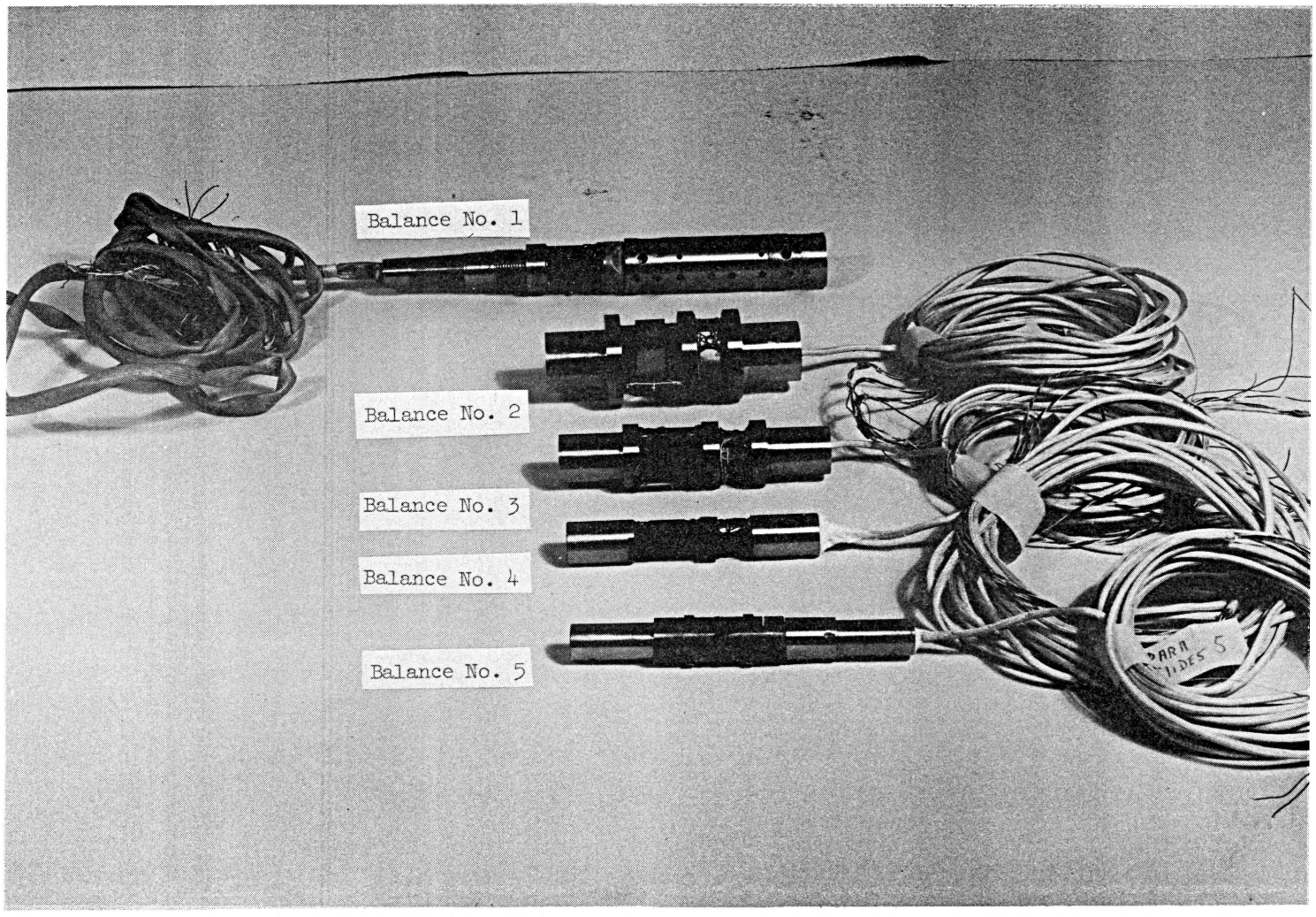

Figure 6.- Load recording balances.

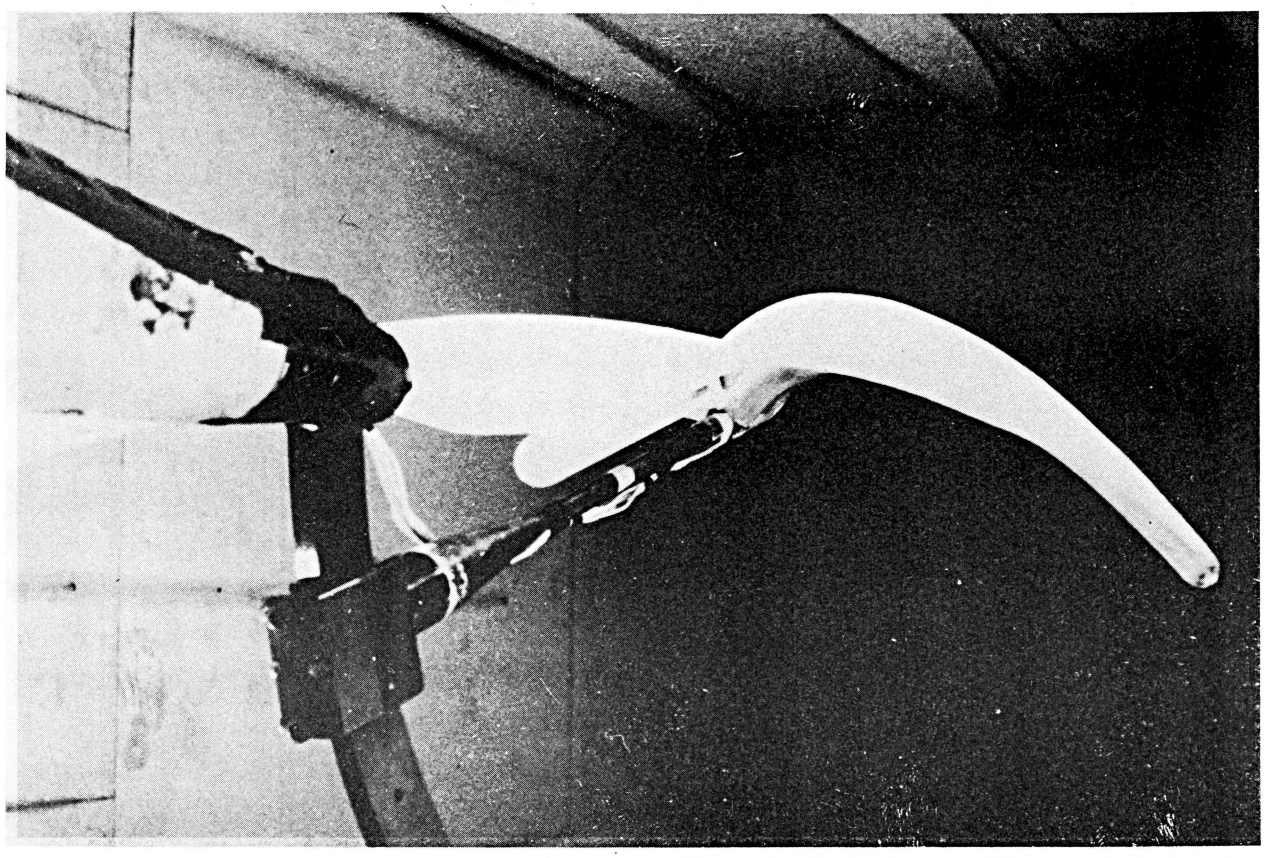

(a) Looking from rear toward apex of paraglider.

Figure 7.- Test model in Langley Research Center 300 mph 7-by-10 ft. wind tunnel facility.

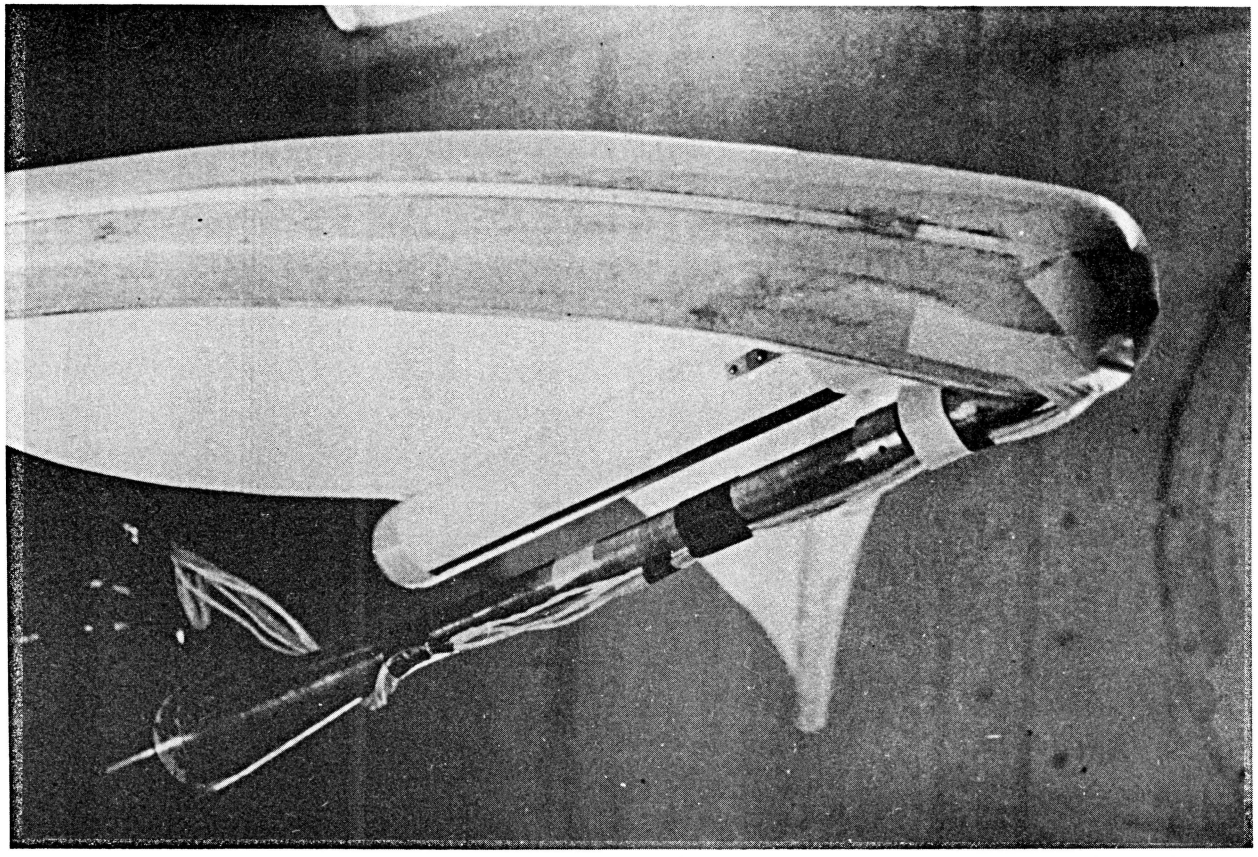

(b) Looking up at the paraglider.

Figure 7.- Continued.

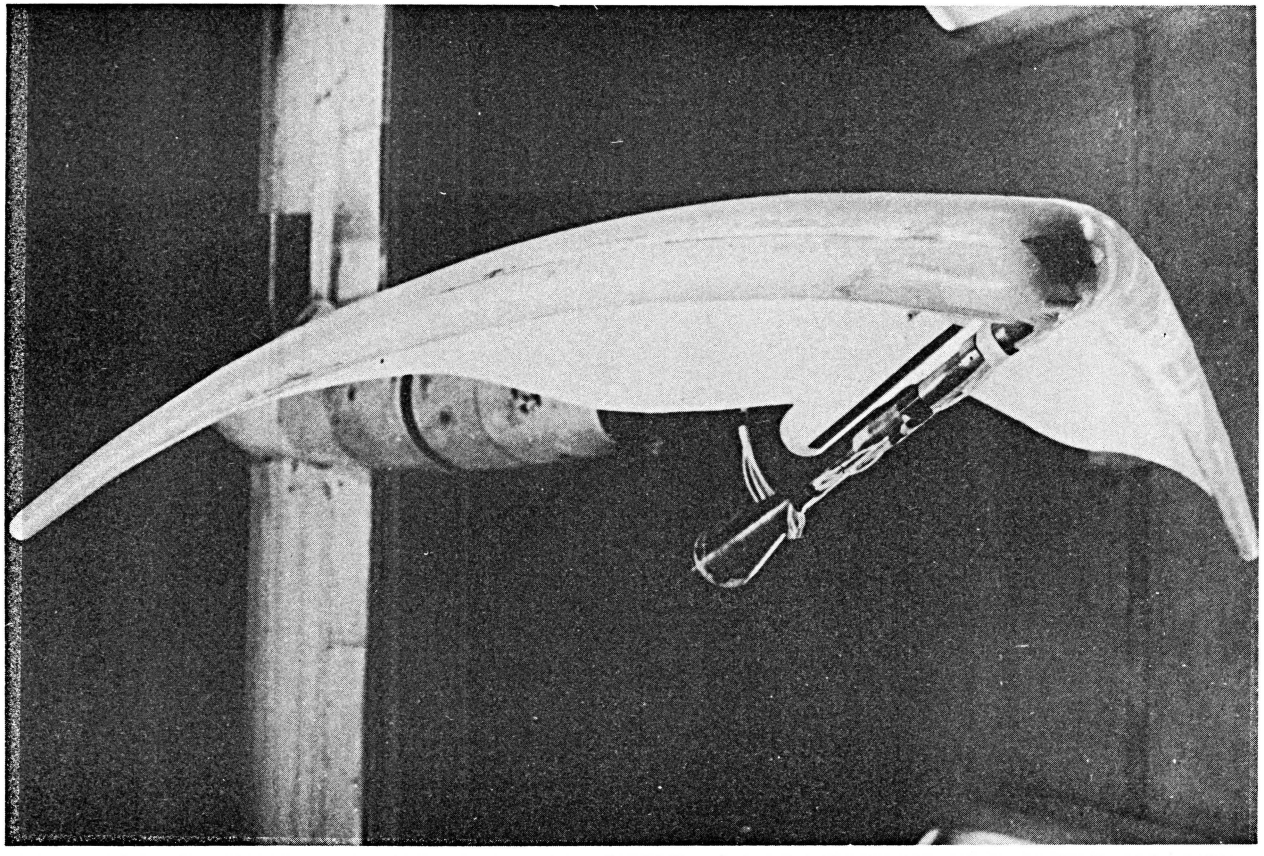

(c) Side view of paraglider.

Figure 7.- Concluded.

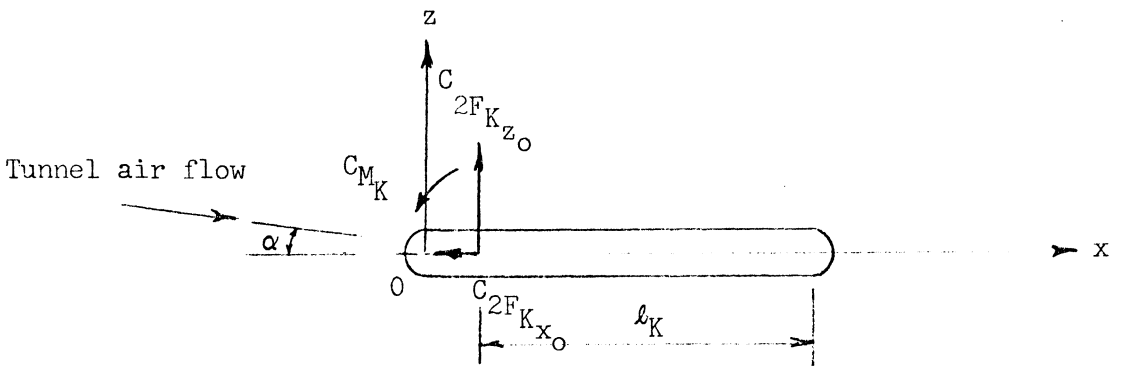

(a) Keel force coefficients shown in their actual sense.

Figure 8.- The recorded keel force coefficients plotted for a q of 5 psf.

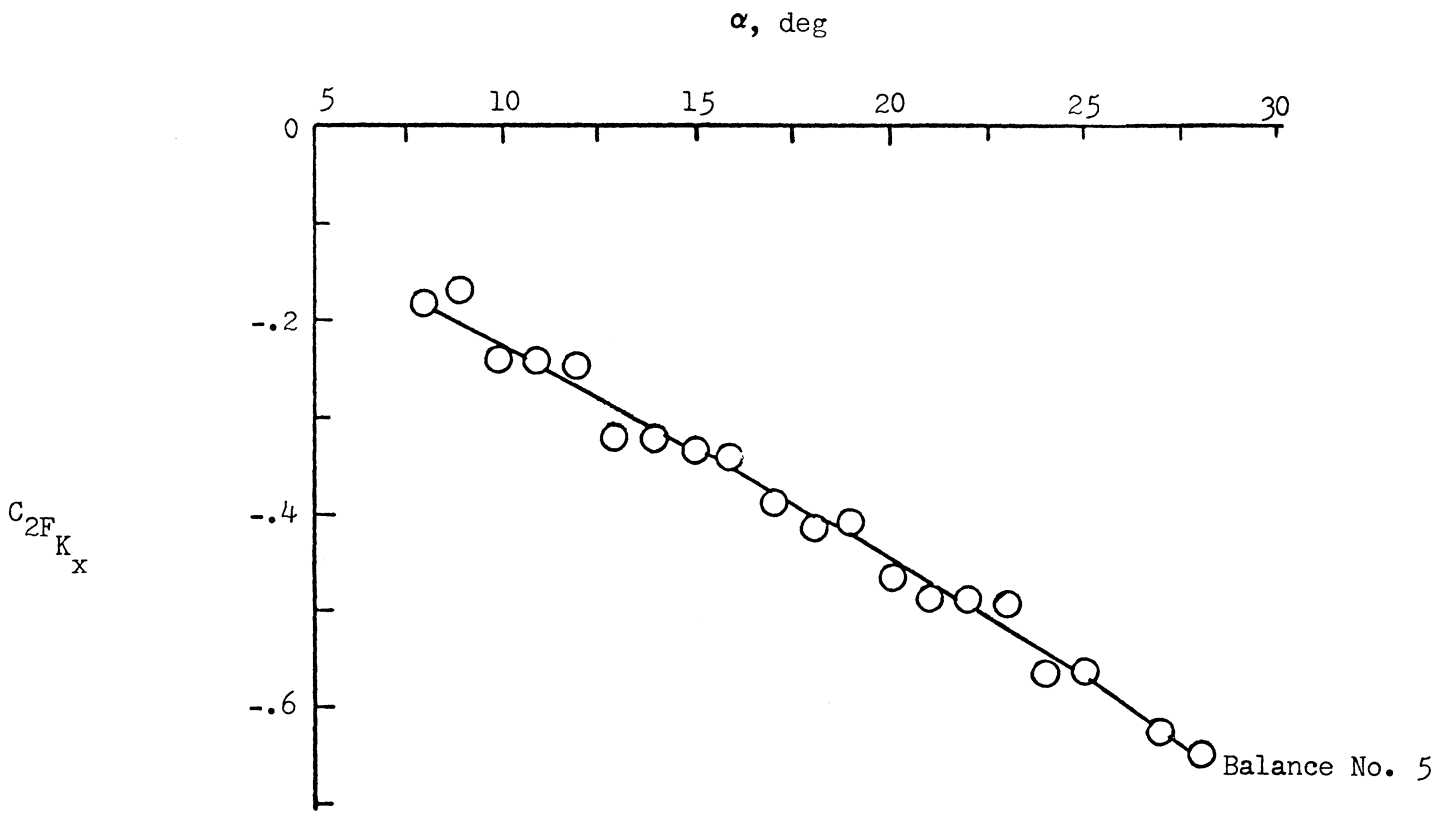

(b) Variation of $C_{2F_{K_x}}$ with angle of attack.

Figure 8.- Continued.

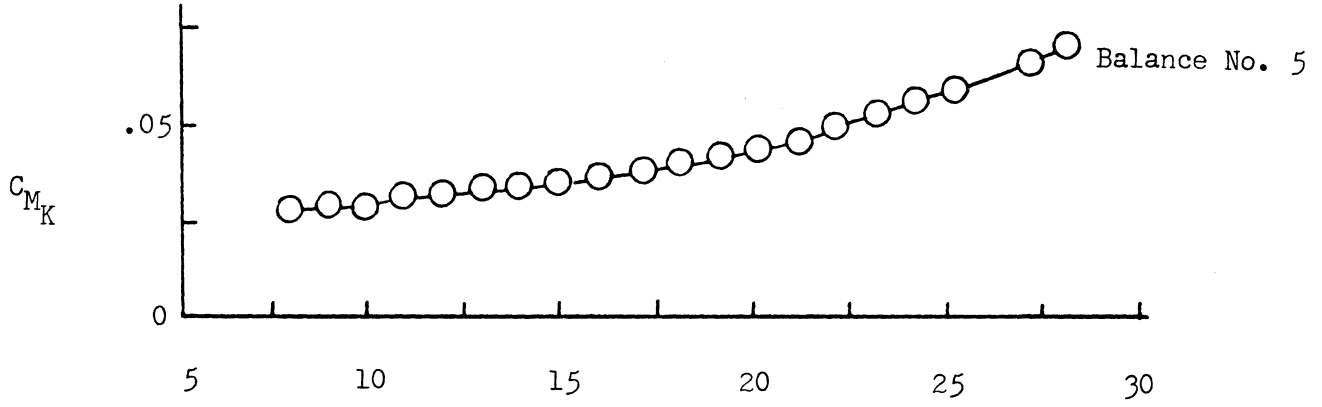

(c) Variation of C_{M_K} with angle of attack.

Figure 8.- Continued.

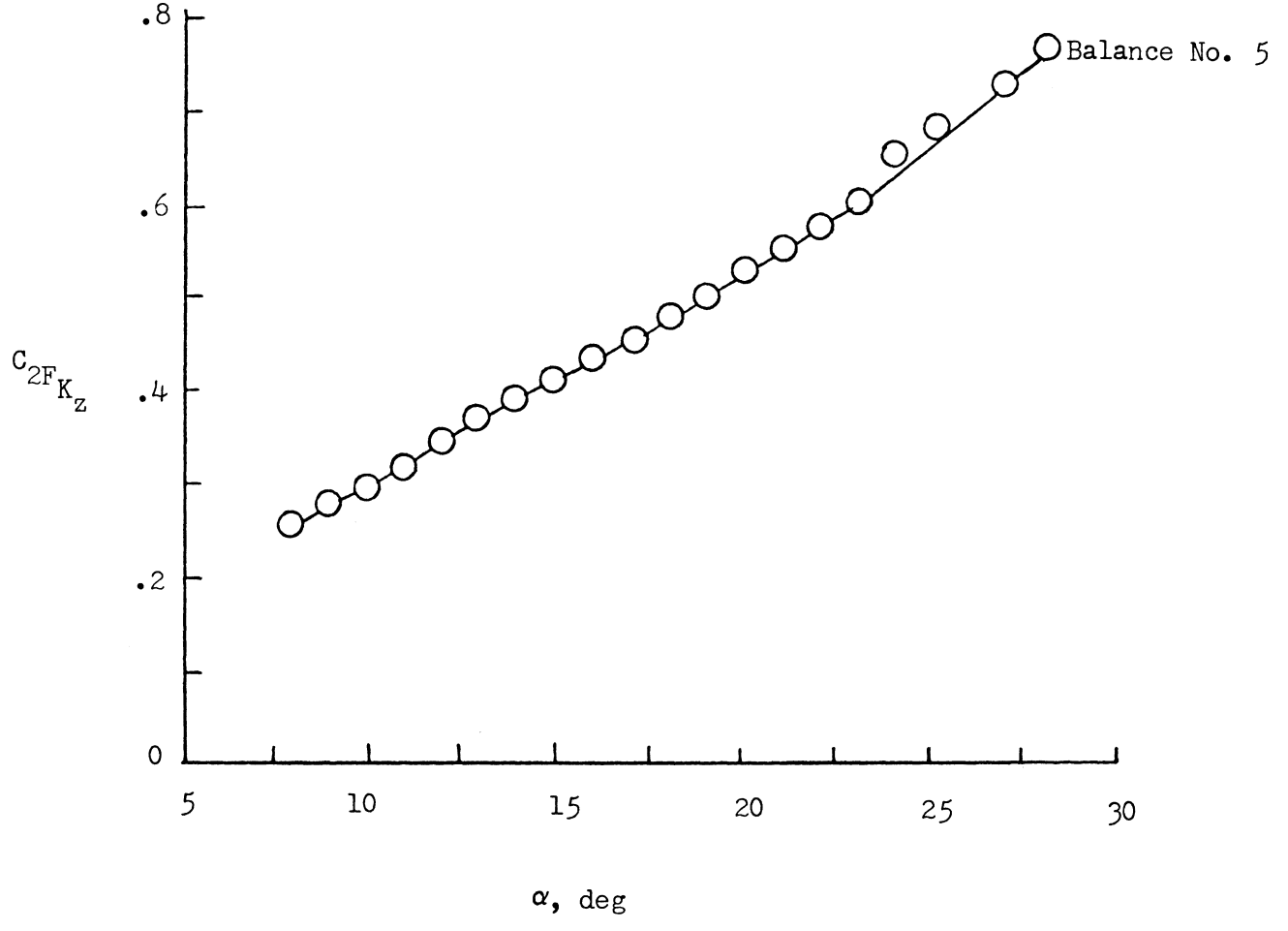

(d) Variation of $C_{2F_{K_z}}$ with angle of attack.

Figure 8.- Concluded.

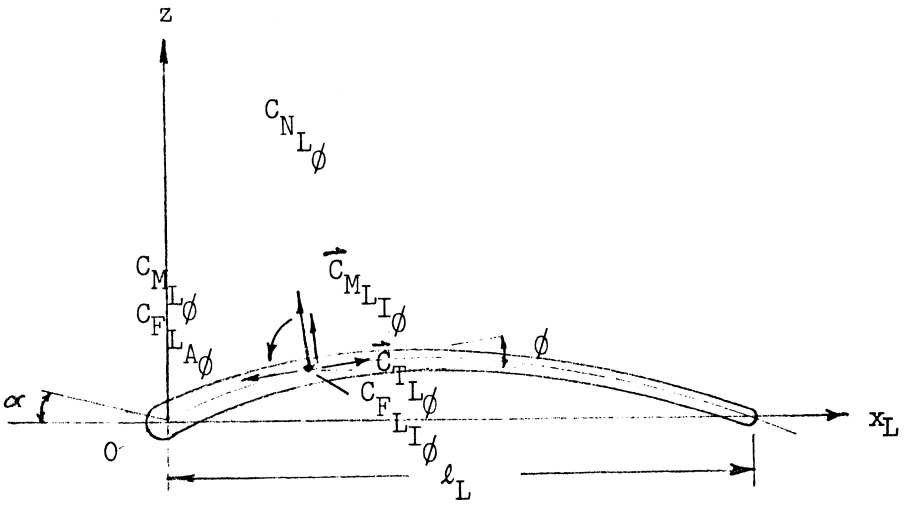

(a) Looking at the paraglider from the rear toward the apex, the above leading edge represents that to the left, and (1) The symbol (⇀) is representative of classical right hand rector notation, (2) $C_{F_{L_{I_\phi}}}$ is represented by a dot, therefore is directed into the paper, and (3) The above leading edge force coefficients are shown in their positive sense.

Figure 9.- The recorded leading edge force coefficients plotted for a q of 5 psf.

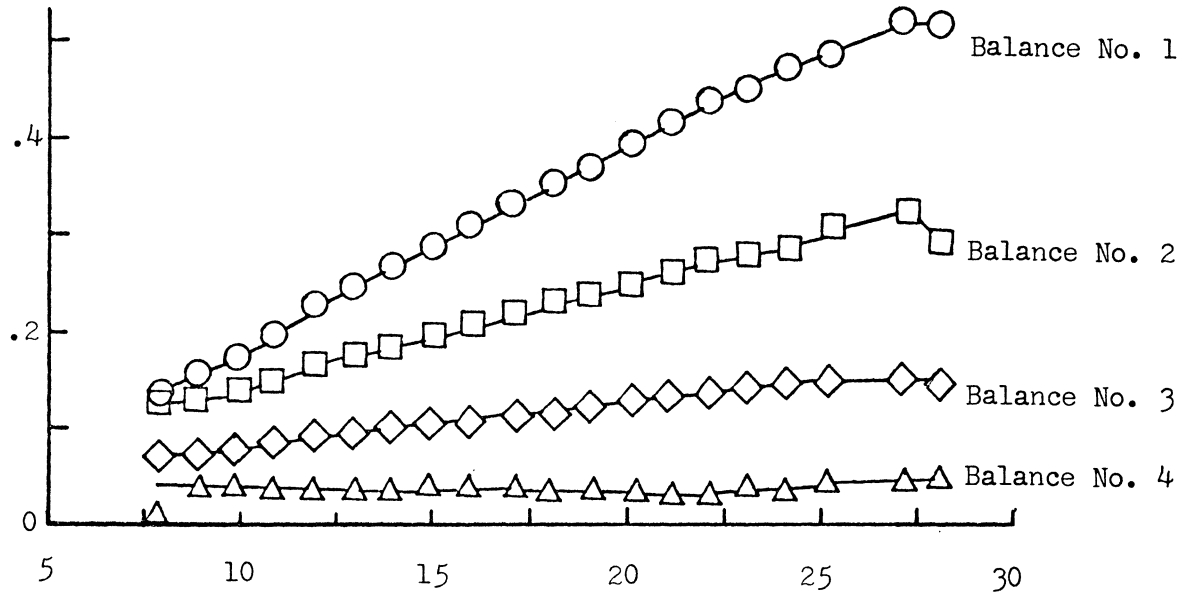

(b) Variation of $C_{N_{L_\phi}}$ with angle of attack.

Figure 9.- Continued.

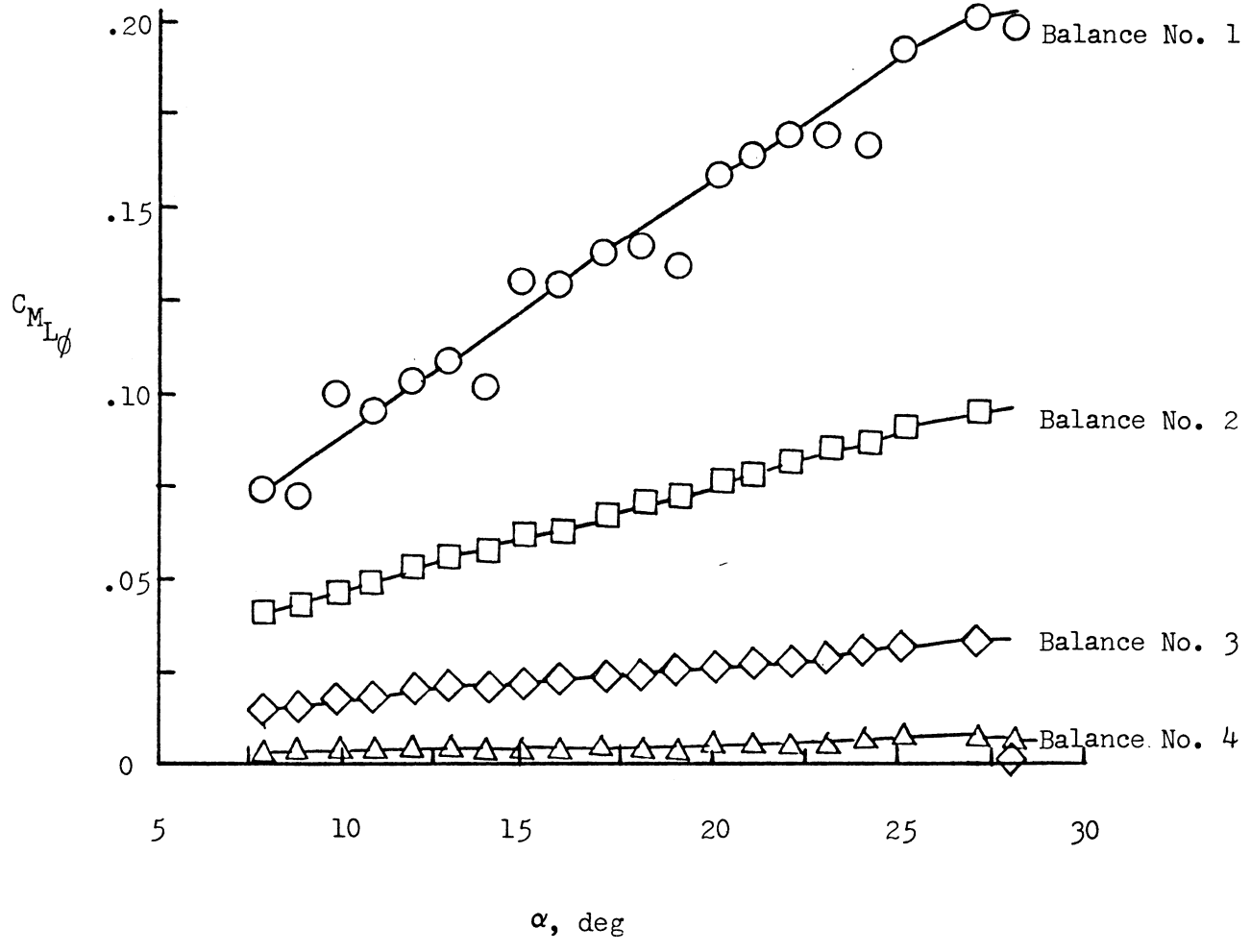

(c) Variation of $C_{M_{L_\phi}}$ with angle of attack.

Figure 9.- Continued.

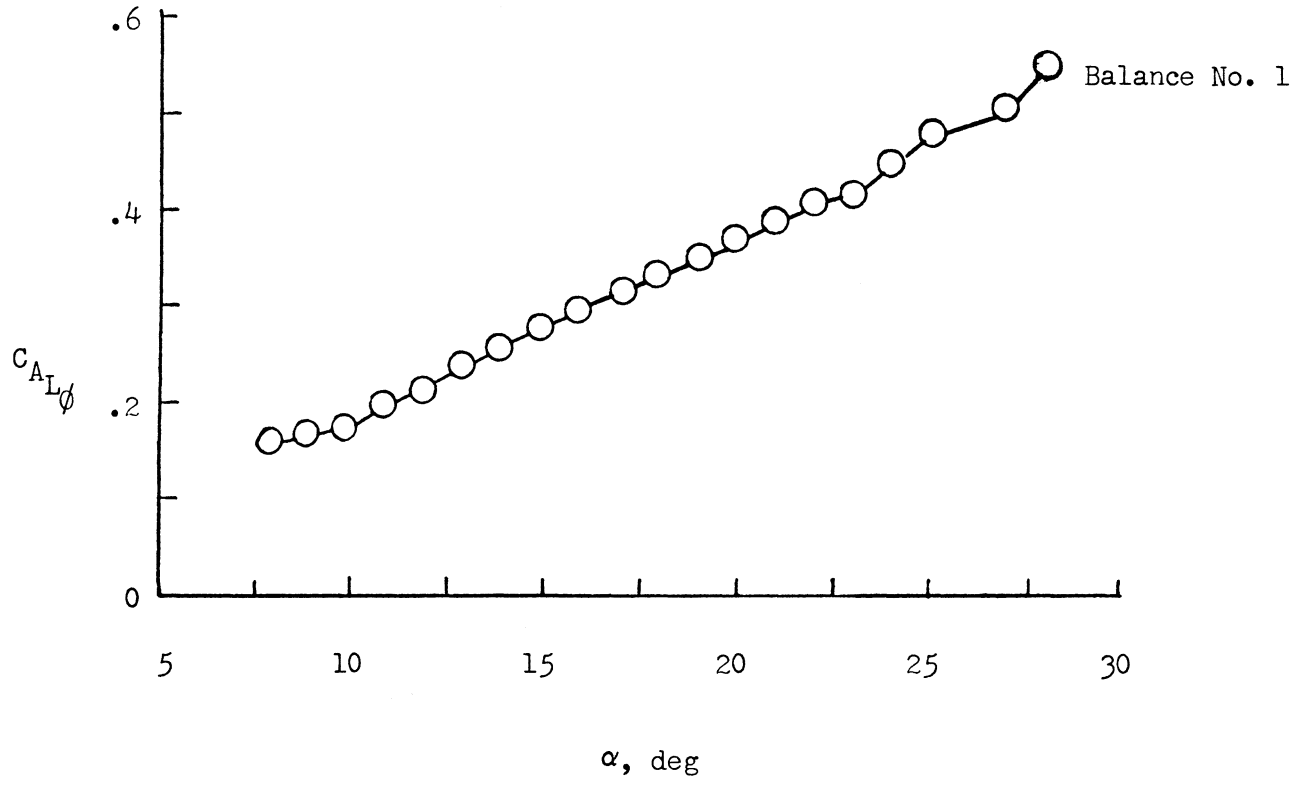

(d) Variation of $C_{A_{L_\phi}}$ with angle of attack.

Figure 9.- Continued.

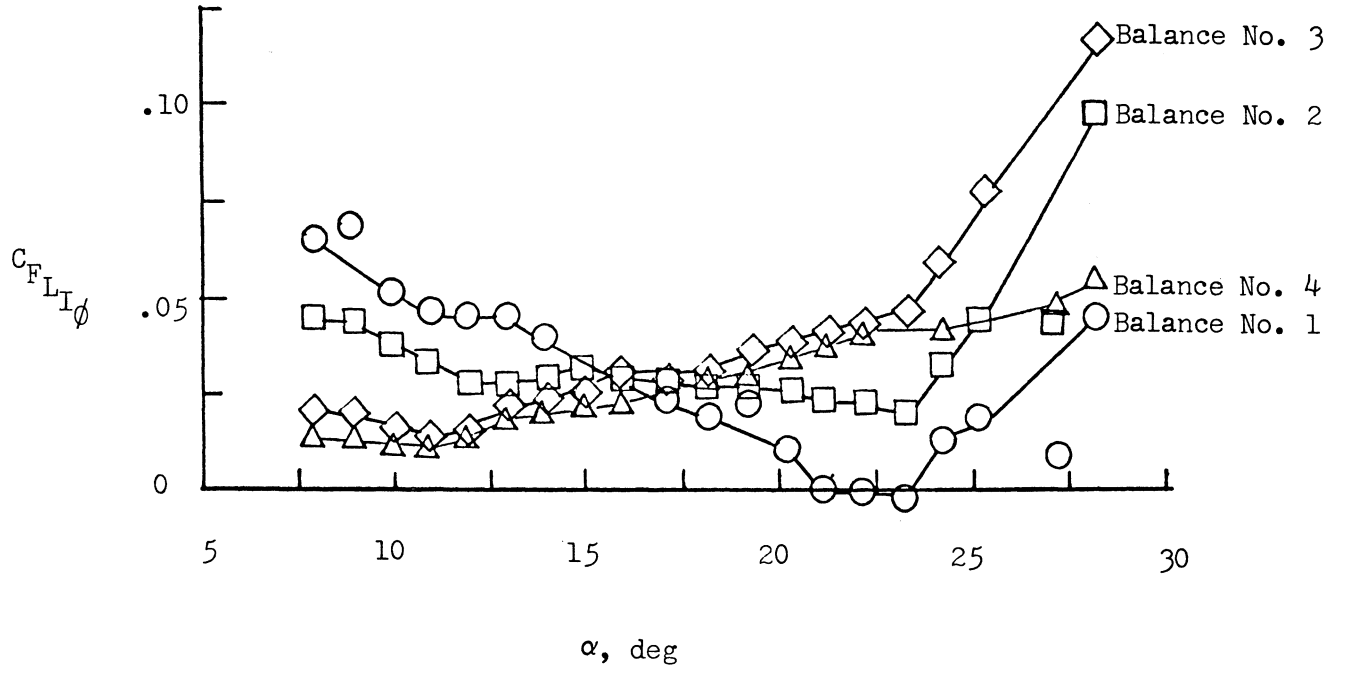

(e) Variation of $C_{F_{L_{I_\phi}}}$ with angle of attack.

Figure 9.- Continued.

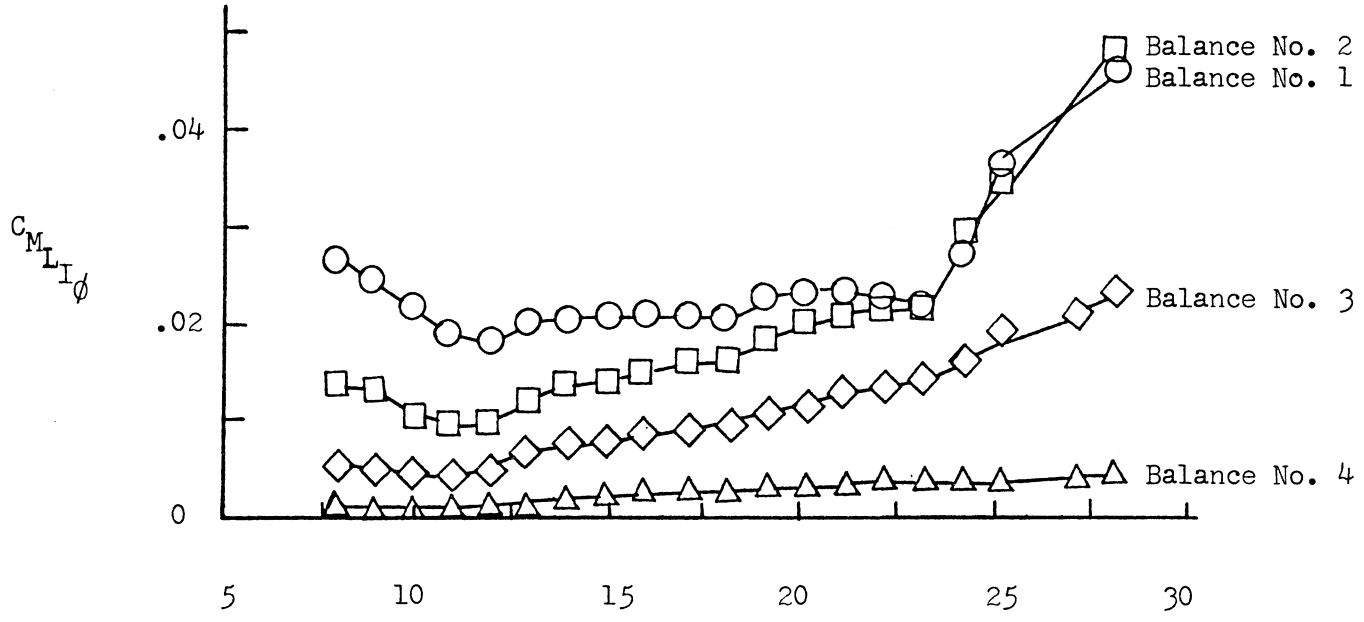

(f) Variation of $C_{M_{L_{I_\phi}}}$ with angle of attack.

Figure 9.- Continued.

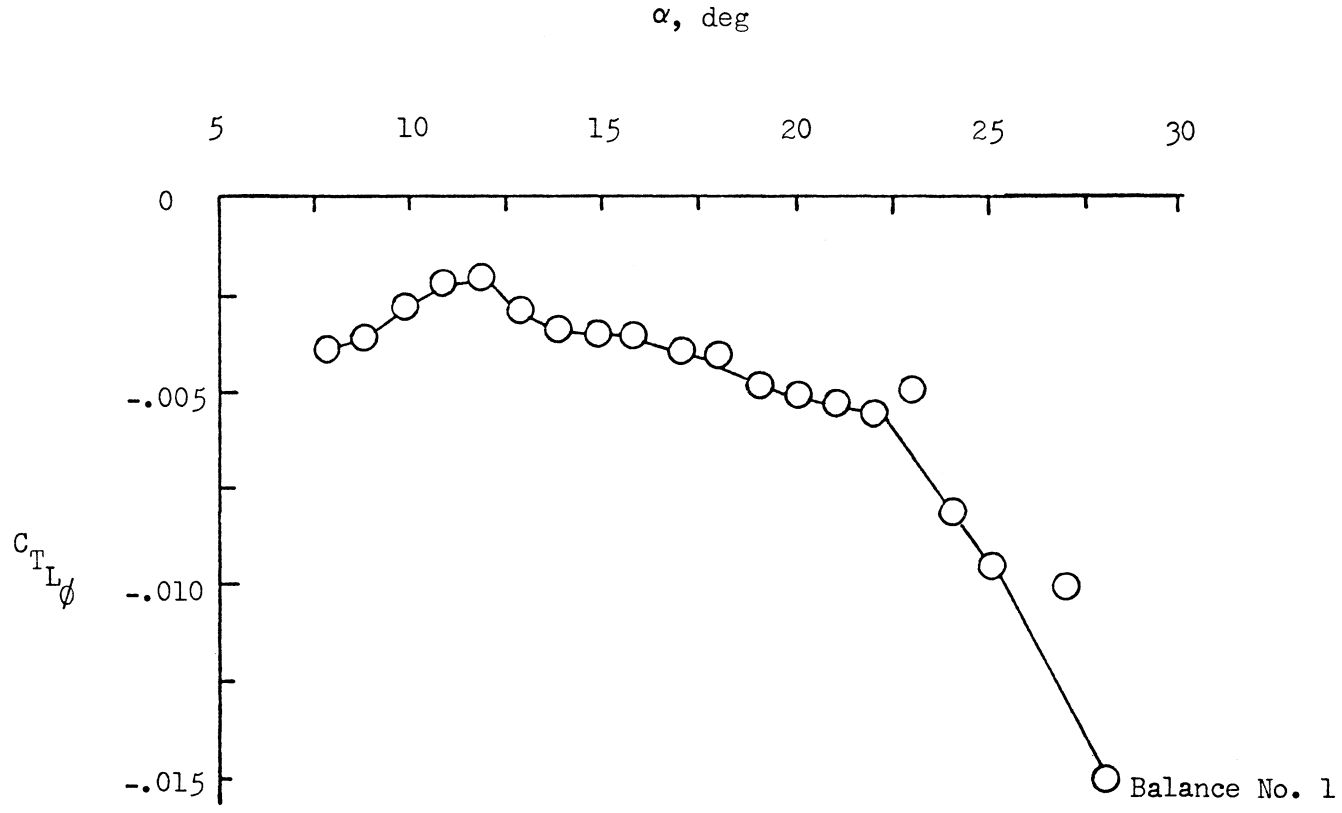

(g) Variation of $C_{T_{L_\phi}}$ with angle of attack.

Figure 9.- Concluded.

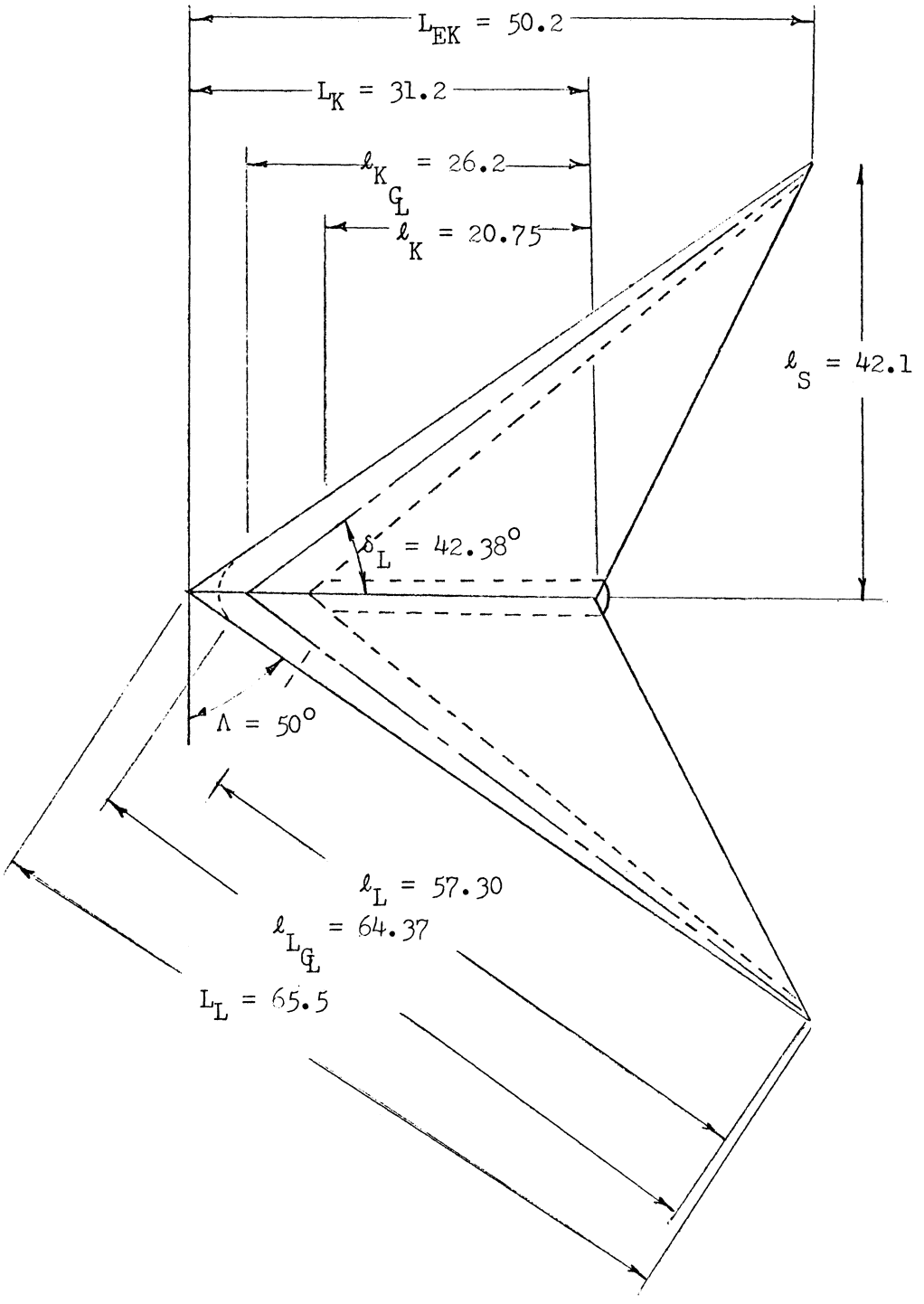

Figure 10.- Layout of paraglider prototype (dimensions in feet).

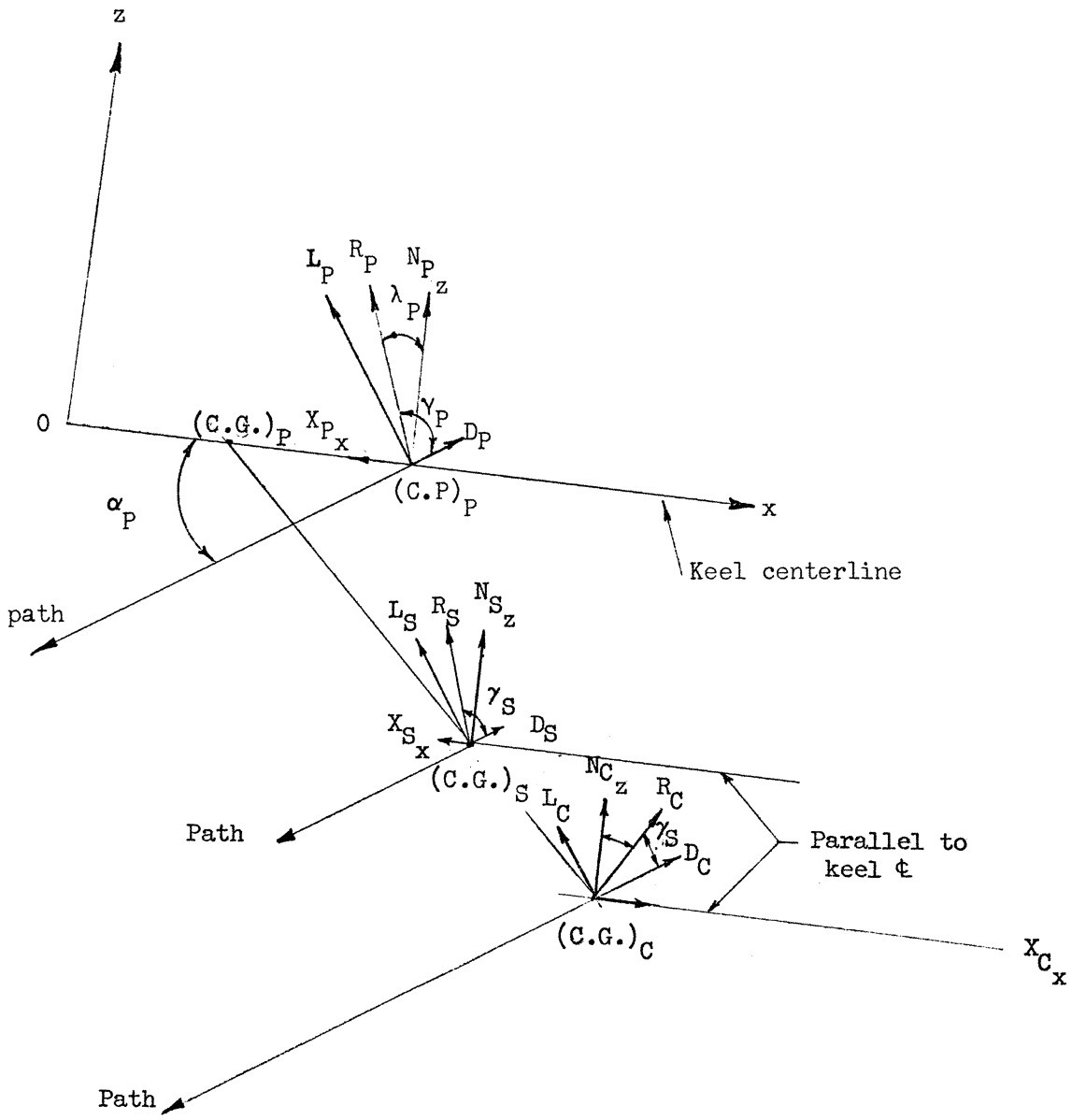

Figure 11.- The paraglider aerodynamic loads geometry.

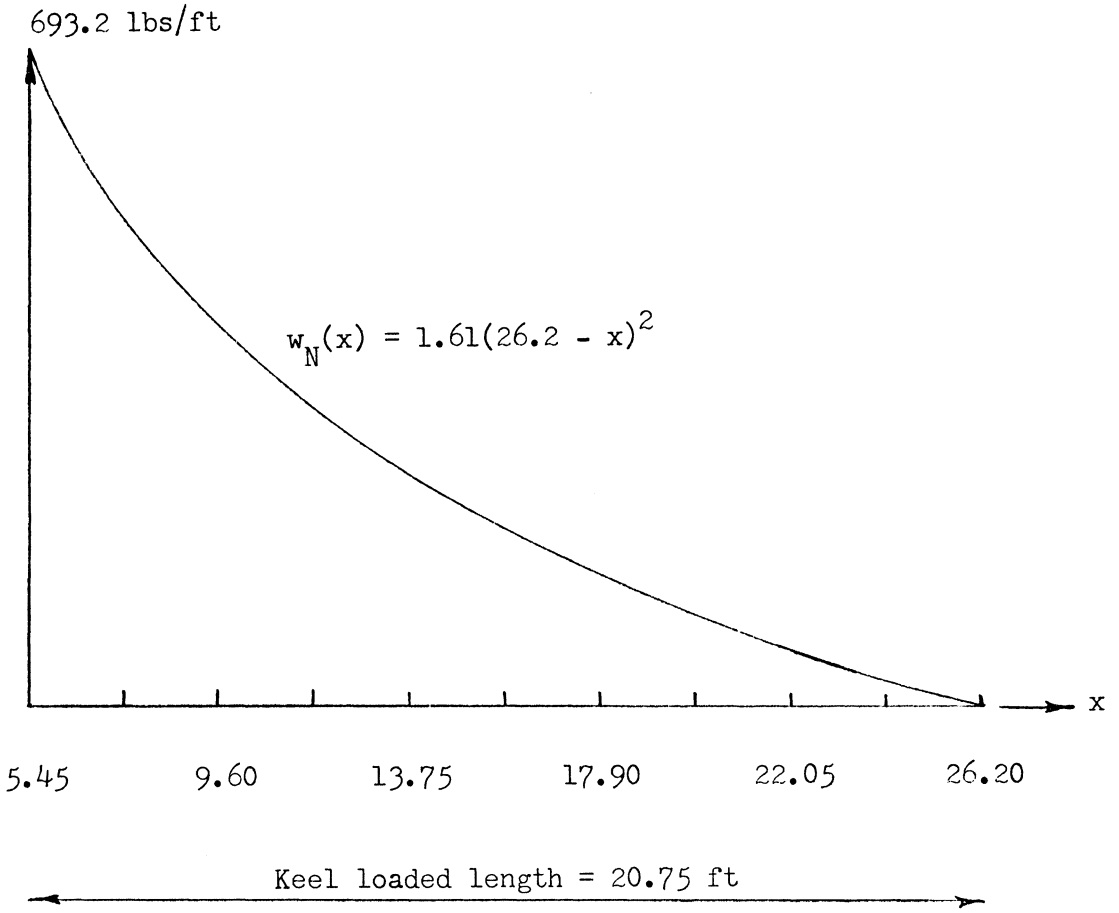

(a) The normal air load component $\left(2F_{K_z}\right)$ distribution over the keel.

Figure 12.- The aerodynamic loads distributed to the prototype paraglider structural members (for a glide angle of attack of 15°) based upon the results of the experimental investigation.

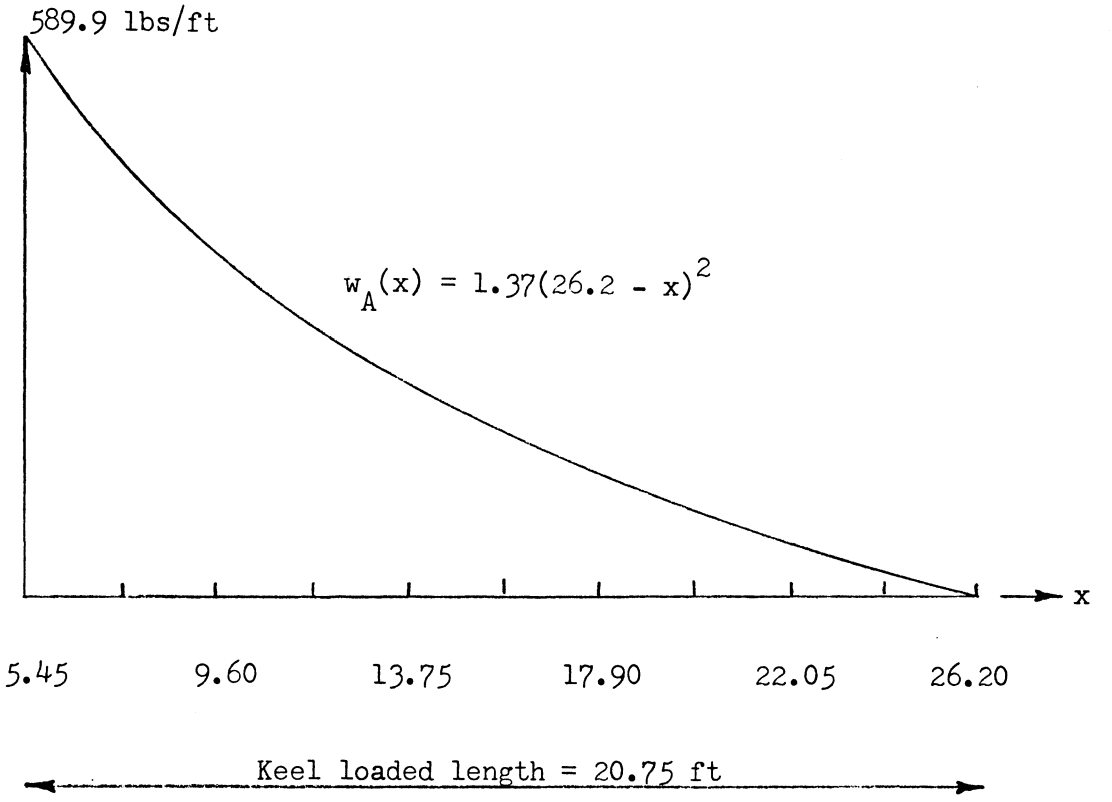

(b) The axially directed air load component $\left(2F_{K_x}\right)$ distribution over the keel (tension).

Figure 12.- Continued.

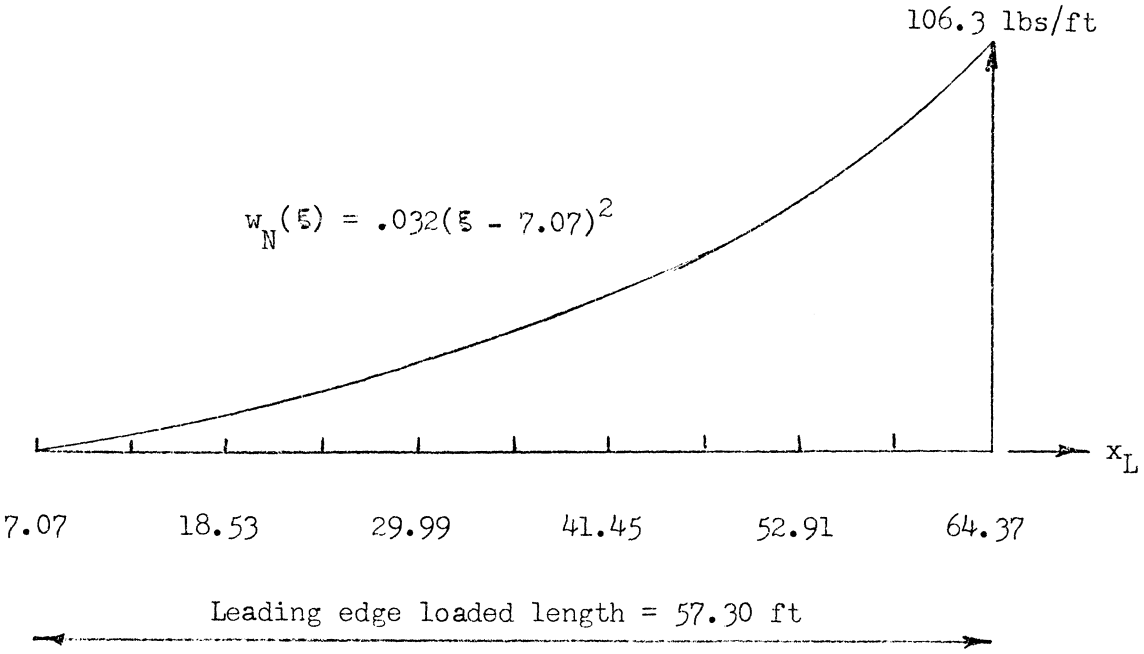

(c) The normal air load component $\left(F_{L_{q_z}} + F_{L_z}\right)$ distribution over the leading edge.

Figure 12.- Continued.

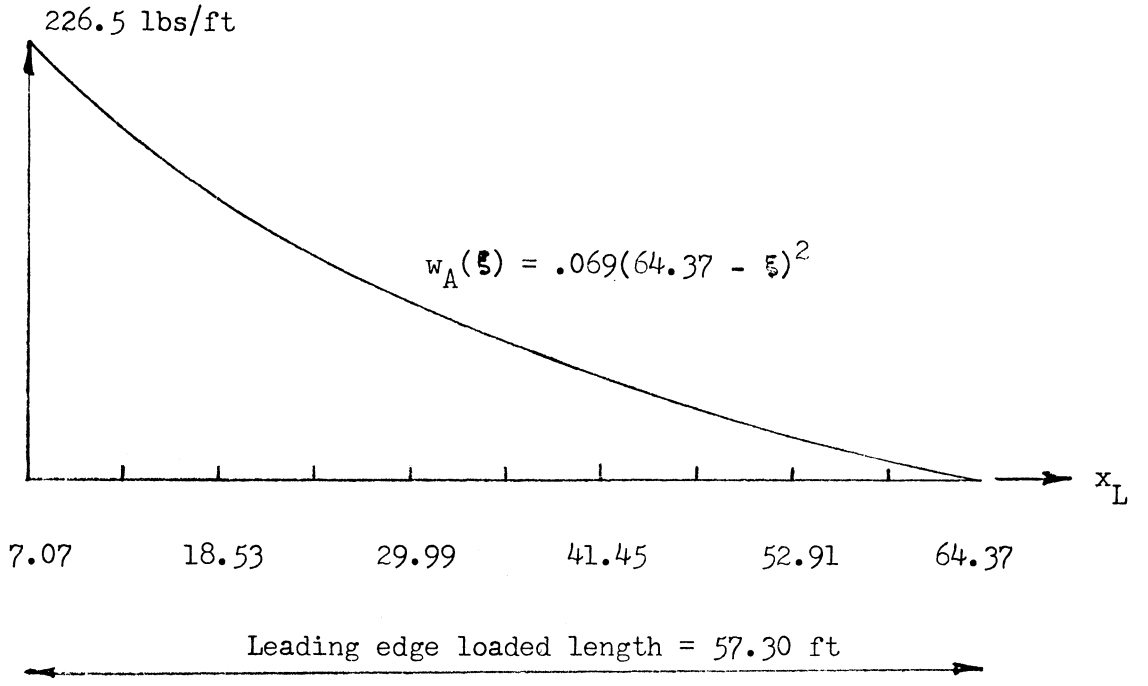

(d) The axially directed load component $\left(F_{L_{A_{x_L}}}\right)$ distribution over the leading edge (compression).

Figure 12.- Continued.

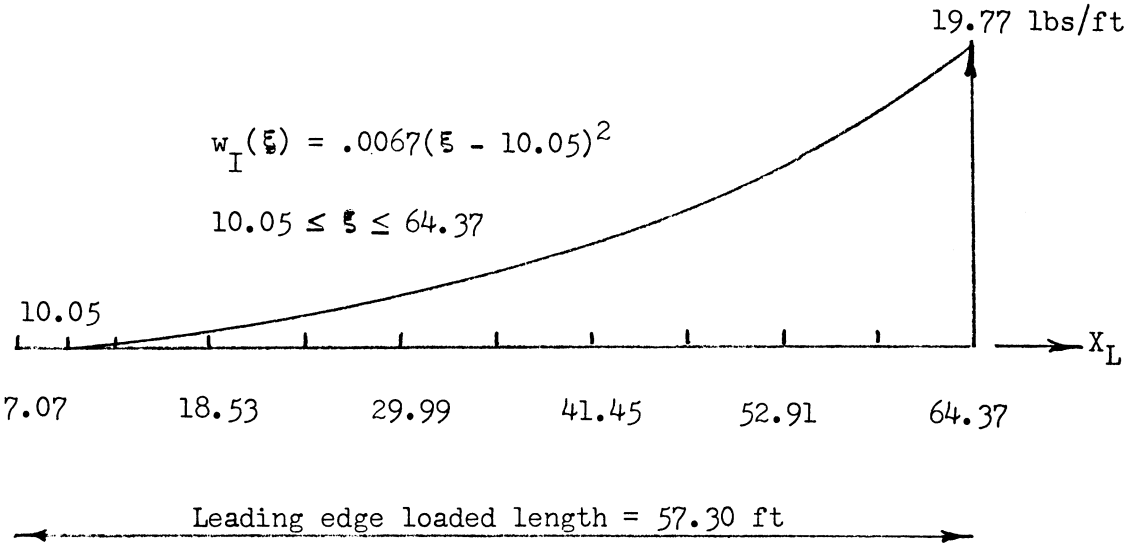

(e) The inboard air load component $\left(F_{L_{q_I}} + F_{L_I}\right)$ distribution over the leading edge.

Figure 12.- Concluded.

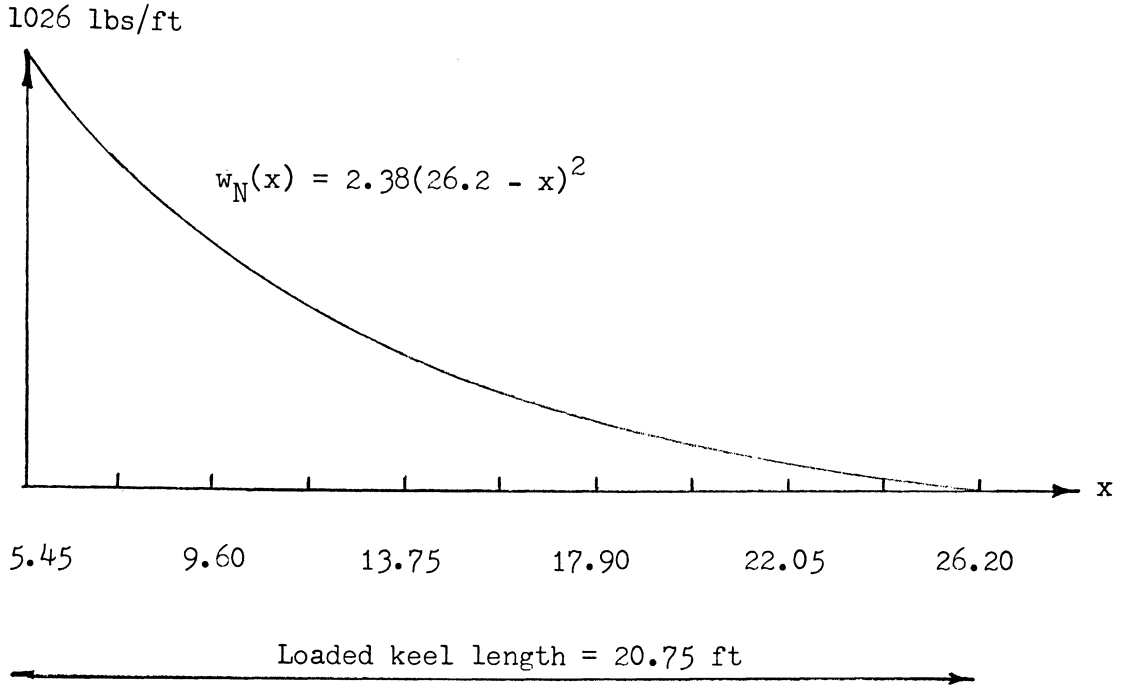

(a) The normal air load component $\left(2F_{K_z}\right)$ distribution over the keel.

Figure 13.- The aerodynamic loads distributed to the prototype paraglider structural members (for a flare angle of attack of 23°) based upon the results of the experimental investigation.

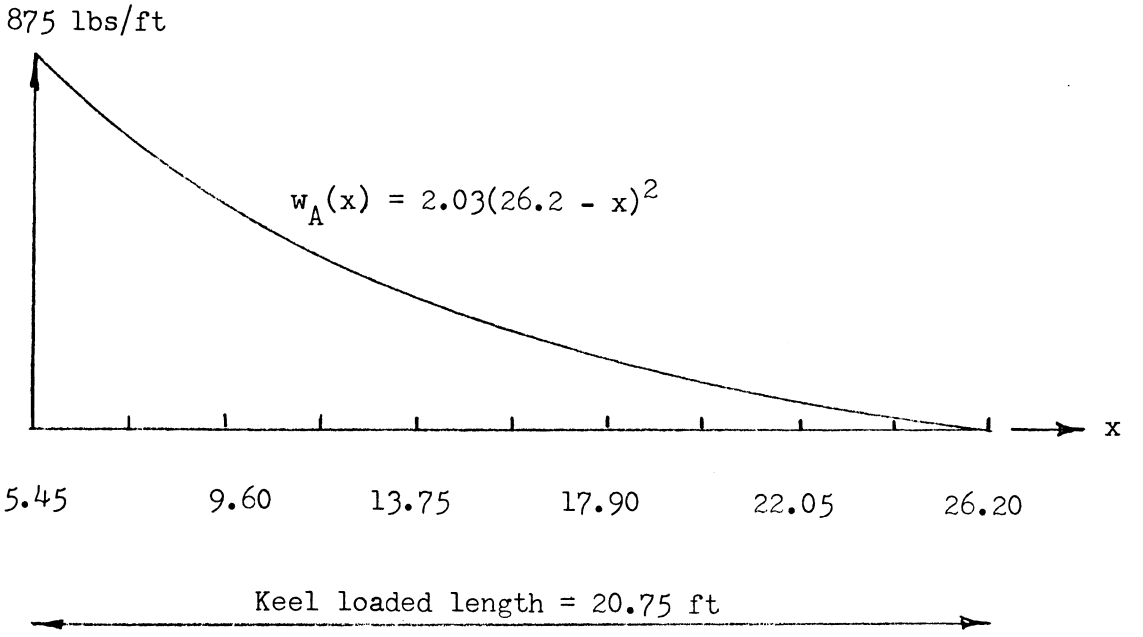

(b) The axially directed load component $\left(2F_{K_x}\right)$ distribution over the keel (tension).

Figure 13.- Continued.

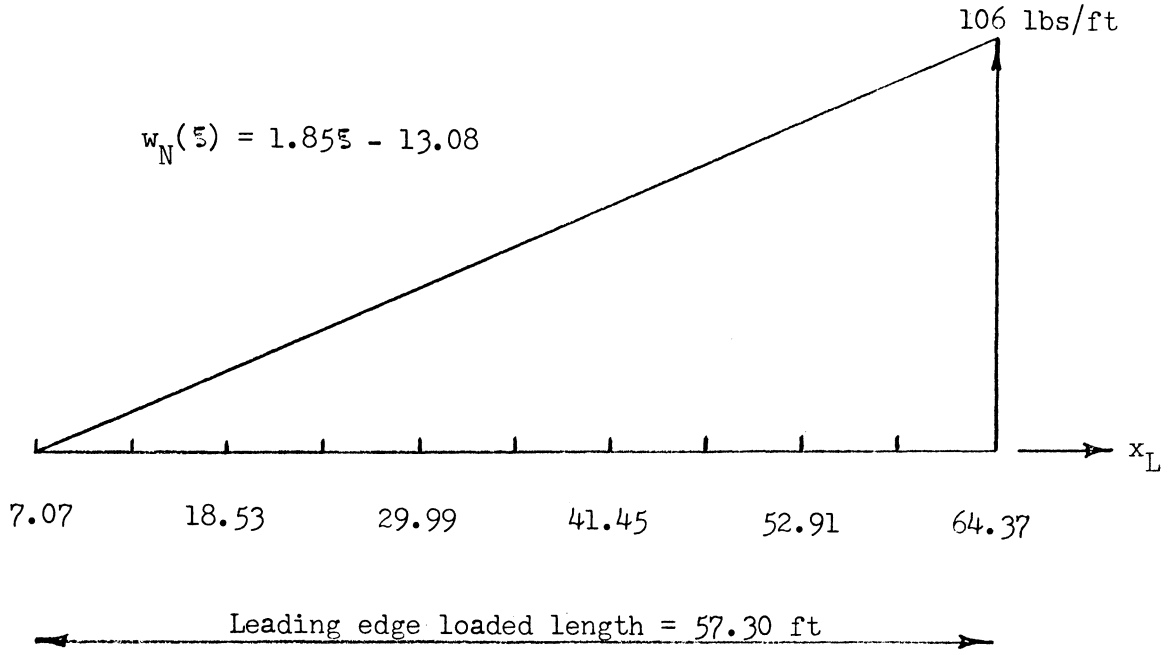

(c) The normal air load component $\left(F_{L_{q_z}} + F_{L_{\dot{z}}}\right)$ distribution over the leading edge.

Figure 13.- Continued.

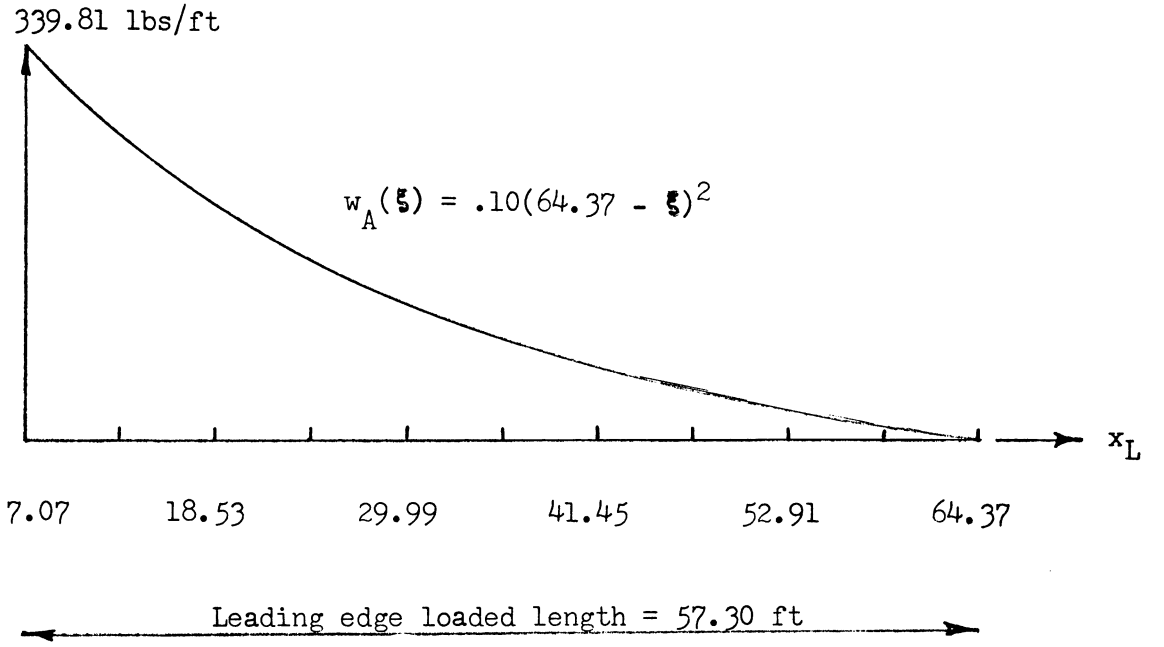

(d) The axially directed load component $\left(F_{L_{A_{x_L}}}\right)$ distribution over the leading edge (compression).

Figure 13.- Continued.

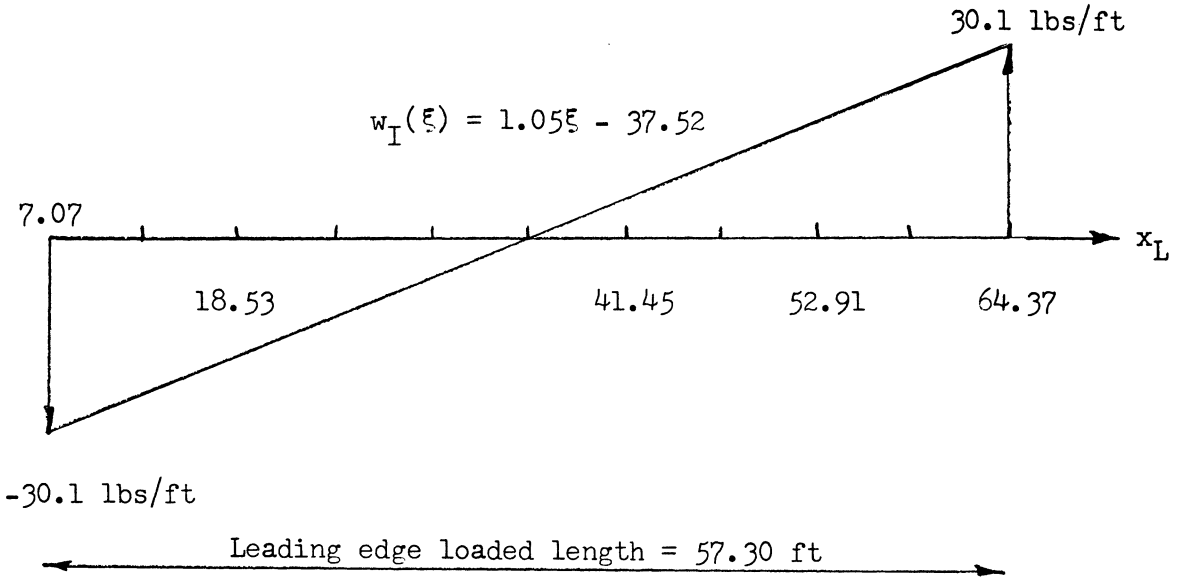

(e) The inboard air load component $\left(F_{L_{q_I}} + F_{L_I}\right)$ distribution over the leading edge.

Figure 13.- Concluded.

TABLE 1

Recorded Test Data for Angles of Attack of 15° and 23°

	$\alpha = 15^\circ$					$\alpha = 23^\circ$				
	Balances					Balances				
	1	2	3	4	5	1	2	3	4	5
$C_{N_{L_\phi}}$	.29	.19	.10	.04	-	.45	.28	.14	.03	-
$C_{M_{L_\phi}}$	.12	.06	.02	.004	-	.18	.085	.03	.005	-
$C_{F_{L_{I_\phi}}}$	.03	.03	.02	.02	-	.045	.040	.028	.000	-
$C_{M_{L_{I_\phi}}}$	.02	.014	.008	.002	-	.002	.021	.014	.004	-
$C_{F_{L_{I_{A_\phi}}}}$	.27	-	-	-	-	.42	-	-	-	-
$C_{T_{L_\phi}}$	-.0035	-	-	-	-	-.0065	-	-	-	-
$C_{2F_{K_{z_o}}}$	-	-	-	-	.40	-	-	-	-	.61
	-	-	-	-	.035	-	-	-	-	.050
$C_{2F_{K_{x_o}}}$	-	-	-	-	-.34	-	-	-	-	-.52

TABLE 2

Aerodynamic Characteristics for Advanced Concept, High Aspect Ratio (5.45) Paraglider
(refer to footnote 1)

	GLIDE	FLARE
α	15°	23°
C_L	.83	1.26
C_D	.108	.25
L/D	7.65	5.05
C_M	.133	.235

TABLE 3

Capsule Aerodynamic Characteristics

α	60°
d	12.83 ft
S	129.3 ft
C_L	0.25
C_D	0.25
(L/D)	1.00
C_M	0.045

AN EXPERIMENTAL INVESTIGATION ON THE DISTRIBUTION OF THE AERODYNAMIC LOADS OVER THE STRUCTURAL MEMBERS OF AN INFLATABLE, HIGH ASPECT RATIO (5.4), ADVANCED CONCEPT PARAGLIDER

By

Royce A. Toni

ABSTRACT

In order to arrive at some "feel" for the aerodynamic loads distributed to the structural members of an advanced concept paraglider at subsonic flight and low aerodynamic pressures, an experimental investigation was initiated and performed at the Langley Research Center.

A paraglider model was designed and fabricated, and load recording balances were inserted within its structural members at various locations. The model was placed into the wind tunnel facility and tested over a range of aerodynamic pressures, where for each pressure the model's angle of attack varied from 5 degrees to 30 degrees.

The test data, collected in terms of force coefficients, was applied to a prototype paraglider system of which the geometry and related aerodynamics are shown in appendix A. The mechanics of the application of the test data to the prototype system is shown in appendix B. The resulting air loads distributions over the structural members for the prototype system for both steady state flight and flare out are shown in figures 12 and 13.